Food Hydrocolloids 180 (2026) 112854

Contents lists available at ScienceDirect

Food Hydrocolloids

journal homepage: www.elsevier.com/locate/foodhyd

Integrated valorisation of protein- and lignin-rich streams from brewers' spent grain through an electrified biorefinery approach for active food packaging applications

Christos Margioulas [a,1], Mirva Sarafidou [a,1], Giovana Colucci [b], Arantzazu Santamaria-Echart [b], Chrysanthi Argeiti [a], Spiros Paramithiotis [c], Theofania Tsironi [a], Apostolis Koutinas [a], Maria-Filomena Barreiro [b,*], Katiana Filippi [a,**]

[a] Department of Food Science and Human Nutrition, Agricultural University of Athens, Iera Odos 75, Athens, 11855, Greece
[b] CIMO, LA SusTEC, Instituto Politécnico de Bragança, Campus de Santa Apolónia, 5300-253, Bragança, Portugal
[c] Laboratory of Microbiology, Department of Biological Applications and Technology, University of Ioannina, 45110, Ioannina, Greece

ARTICLE INFO

Keywords:
Brewers' spent grain
Bacterial cellulose
Lignin
Protein
Food packaging

ABSTRACT

This work highlights the potential of valorising brewing industry side-streams for the development of bio-based food packaging materials. Brewers' spent grain (BSG) was pre-treated using a non-thermal air-bubble plasma reactor as part of an electrified biorefinery, followed by enzymatic hydrolysis, enabling the separation of protein-, lignin-, and sugar-rich fractions. The residual solids (BSG-RS) were explored through three film-forming strategies, with the film formulation using the recovered protein concentrate emerging as the most efficient process. This route was further optimised by incorporating bacterial cellulose nanostructures, produced from the sugar-rich hydrolysate, as a reinforcing agent. Delignification of BSG-RS enabled the recovery of a lignin-rich fraction, which was used to enhance film functionality by testing two lignin formulations, namely alkaline lignin (AL) and lignin particles (LPs). The developed films exhibited excellent light-barrier properties (T_{600} < 2.3 %) and high antioxidant activity (>38.2 % inhibition). Structural characterization (scanning electron microscopy, thermogravimetric analysis, and X-ray diffraction) demonstrated distinct morphology-dependent interactions of the AL and LPs within the film matrix, leading to opposite effects on structural organisation and thermal stability. When applied to refrigerated salmon fillet, selected formulations performed comparably to PVC and extended shelf life by up to 4 days. Overall, the proposed approach effectively valorised all derived fractions of the BSG-based biorefinery towards functional food packaging, contributing to the sustainable utilisation of industrial side-streams into eco-friendly alternatives to conventional packaging.

1. Introduction

Conventional food packaging depends on fossil-based plastics, which are non-biodegradable and environmentally harmful, contributing to greenhouse gas emissions and long-term ecological degradation (Boarino & Klok, 2023; X. Li et al., 2025). In 2023, global plastic production reached 413.8 Mt, highlighting the urgent need for sustainable alternatives (Statista, 2025). At the same time, the growing accumulation of agro-industrial side streams intensifies environmental pollution, highlighting the necessity for effective valorisation strategies (Yin & Woo, 2024). In line with circular economy principles, converting biomass feedstocks into high-value biopolymers enables their reintegration into sustainable food packaging systems (Yin & Woo, 2024).

Brewers' spent grain (BSG) represents approximately 30 % (w/w) of malt weight and up to 85 % of total brewery residues (Tsouko et al., 2023). The production of 1 m^3 of beer results in approximately 270 kg of solid waste, with more than 10.8 million t of BSG generated in Europe (Ioannidou et al., 2020). BSG can be classified as a lignocellulosic material, consisting of hemicellulose (20-40 %), cellulose (12-30 %), protein (14-46 %) and lignin (12-28 %) (Argeiti et al., 2024; Tsouko et al.,

* Corresponding author.
** Corresponding author.
E-mail addresses: barreiro@ipb.pt (M.-F. Barreiro), filippi@aua.gr (K. Filippi).
[1] Equally contributed as first authors.

https://doi.org/10.1016/j.foodhyd.2026.112854
Received 23 November 2025; Received in revised form 14 April 2026; Accepted 4 May 2026
Available online 5 May 2026

2023). BSG-based biorefineries have been reported for the isolation of different value-added products, such as bioactive compounds (Bonifácio-Lopes et al., 2020), arabinoxylan (López-Linares et al., 2020), proteins (Devnani et al., 2023), the biotechnological production of poly (3-hydroxybutyrate) (PHB) (Argeiti et al., 2024), bacterial cellulose (BC) (Tsouko et al., 2023), and various chemicals (e.g., butanol, xylitol, lactic acid, ethanol and biogas) (Rojas-Chamorro et al., 2020; Sganzerla et al., 2021). However, its recalcitrant structure requires pre-treatment before enzymatic saccharification (Vanneste et al., 2017). Conventional hydrothermal or alkaline pre-treatments involve high energy input and chemical reagents, leading to inhibitor formation and product loss. Recent studies on biorefinery electrification have demonstrated that non-thermal air-bubble plasma (NTP) offers a sustainable alternative, operating at ambient temperature and pressure, without acids or solvents. The reactive oxygen and nitrogen species generated in plasma (such as •OH, O_3, and NO_3^-) promote lignin depolymerisation and cell wall disruption, enhancing enzymatic hydrolysis yields. Applied to BSG and grape stalks, NTP enhanced enzymatic hydrolysis, while a life-cycle assessment confirmed a lower environmental impact than conventional thermochemical pre-treatments (Argeiti et al., 2024; Filippi et al., 2025).

Natural polymers provide a renewable platform for the production of biodegradable films and coatings (Gupta et al., 2022). BSG-derived proteins serve as a low-cost nitrogen source with strong intermolecular interactions and promising oxygen barrier properties (Rojas-Lema et al., 2023). They have been utilised in human and animal dietary (Devnani et al., 2023; Junttila, 2022), and in packaging formulations (Oztuna Taner et al., 2023; Proaño et al., 2020; Shroti & Saini, 2022).

Lignin, one of the most abundant natural biopolymers, is mainly generated as a by-product of agricultural industries (Lu et al., 2022). Its hydrophobicity makes it a suitable reinforcing agent for protein-based films, improving moisture resistance (Rojas-Lema et al., 2023). However, its random structure and low solubility limit direct use. To overcome this limitation, lignin particles (LPs) incorporation has emerged as a promising approach to enhance antioxidant, antimicrobial, UV-barrier, and thermal properties of the films (Lu et al., 2022). Incorporating BC into this framework introduces a high-purity, crystalline biopolymer that outperforms plant cellulose in film reinforcement and in compatibility with protein matrices (Gregory et al., 2021; Sarafidou, Forys, et al., 2025). Its integration within a biorefinery context can reduce production costs and expand applications (Filippi et al., 2022). Further acid hydrolysis of BC yields bacterial nanocellulose (BNC) which acts as an efficient reinforcing agent in protein-based films, enhancing mechanical strength and barrier properties (Efthymiou et al., 2022a).

Previous studies have developed BSG-based packaging materials using bio-based blends. Rigid food packaging trays made from BSG and potato starch exhibited mechanical properties comparable to those of expanded polystyrene (Ferreira et al., 2019). Shroti and Saini (2022) investigated the effect of different BSG protein contents (4-10 % wt.%) and pH values (11, 12 and 13) on the formation of edible films, while Proaño et al. (2020) produced BSG protein concentrate (BSG-PC) films through solubilisation at different pHs (2, 8, 11) and plasticised with polyethylene glycol or glycerol for active packaging. Nanocomposite films formulated using BSG feruloylated arabinoxylo-oligosaccharides with the addition of nanofibrillated cellulose were reported by Moreirinha et al. (2020), leading to high UV-Vis barrier, antioxidant and antimicrobial properties. All these studies utilised pure components derived from different sources or have only valorised a part of the BSG biomass, leaving the remaining streams unutilised. Oztuna Taner et al. (2023) developed BSG-derived films for strawberry packaging by combining a cellulose derivative (carboxymethyl cellulose), with protein and phenolic compounds from BSG, with the disadvantage of using a chemical modification. Qazanfarzadeh et al. (2024) developed a cascade biorefinery process to valorise the protein-, cellulose-, and hemicellulose-rich BSG streams into films for blueberry preservation. However, no study has yet examined the processing of residual BSG following NTP treatment within an electrified biorefinery framework aimed at producing active food packaging, nor has any application on actual food products been reported. Moreover, the use of high-purity BNC produced directly from BSG hydrolysates, an approach that avoids plant-derived cellulose and chemical derivatization, has not been explored so far.

This study aims to demonstrate that all major fractions from BSG obtained through an electrified biorefinery approach can be efficiently converted into bio-based packaging materials. The work investigates whether BSG after pre-treatment in a plasma-bubble bioreactor, followed by enzymatic hydrolysis enables the valorisation of protein-, lignin-, and sugar-rich streams suitable for film development. Different utilisation strategies for the residual solids, either directly or after protein and lignin fractionation, were evaluated to identify the most efficient route for producing robust films. Additional research quest addresses the ability of two different lignin forms (alkaline lignin or LPs) to enhance film functionality. The resulting BSG-based film's performance was assessed using refrigerated salmon fillets as a case study to determine their suitability as sustainable packaging materials.

2. Materials and methods

2.1. Raw material

BSG (Cerveza Mica, Spain) was collected after the malting step of Pilsner beer. Wet BSG was milled using a blender (particle size <2 mm) and stored at −20 °C until further processing.

2.2. Pre-treatment by air-bubble plasma reactor and enzymatic hydrolysis

BSG was pre-treated using an air-bubble plasma reactor (Leap100, Plasmaleap, Sydney, Australia) at atmospheric pressure, following the optimised conditions described by Argeiti et al. (2024). The plasma reactor consists of a ground electrode (cathode), a high-voltage electrode (anode) sealed in a quartz tube with an air supply, an AC power supply unit and an agitator. The reactor configuration enabled both dielectric barrier discharge (DBD) and spark discharges within the gas bubbles, enhancing the transfer of reactive species to the liquid phase.

A 150 g/L BSG suspension (0.9 L working volume) was treated at 200 V, a discharge frequency of 1000 Hz, a 10 % duty cycle (100 μs pulse width) for 30 min under continuous aeration (1 vvm) and agitation at ambient temperature. The duty cycle was defined as the ratio of pulse width to discharge period (T). The discharge period was calculated according to equation (1).

$$T = \frac{1}{f} \quad (1)$$

where f is the discharge frequency (Hz).

Enzymatic hydrolysis of the whole plasma-treated suspension was performed immediately after pre-treatment. A commercial enzyme cocktail (ASA Spezialenzyme GmbH, Wolfenbüttel, Germany) containing glucoamylase, cellulase and xylanase was added at 100 μL per g BSG under aseptic conditions. Hydrolysis was performed at 50 °C for 48 h with agitation. After hydrolysis, residual solids (BSG-RS) were separated from the hydrolysate and stored at −20 °C.

2.3. BSG-RS processing strategies

BSG solids after NTP treatment and enzymatic hydrolysis were subjected to two processing strategies: direct film formulation utilising BSG-RS (the basis of treatments 1 and 2) and protein extraction followed by film formulation (treatment 3).

2.3.1. Treatment of BSG-RS with mild acid hydrolysis (treatment 1)

BSG-RS suspensions (5 %, 7.5 %, and 10 %) were prepared in 1 M acetic acid and stirred at 400 rpm for 24 h according to the protocol described by Merino et al. (2021).

2.3.2. Organosolv (acetic acid) treatment of BSG-RS (treatment 2)

BSG-RS (1:10 w/v) was suspended in aqueous acetic solution (70 %, 80 %, and 90 % v/v) in Duran bottles, followed by the addition of 2 % v/v HCl as a catalyst, as reported by De Sousa Nascimento et al. (2021) to effectively solubilise lignin from lignocellulosic residues. Suspensions were heated under stirring to 110 °C for 1 h in a silicon oil bath, resulting in the formation of black liquor.

2.3.3. Alkaline treatment – protein extraction (treatment 3)

BSG-RS was dispersed (1:10 w/v) and adjusted to pH 10.0 with 5 M NaOH. The slurry was stirred for 2 h (Witeg MSH-D, Germany) at 60 °C, whereas the pH was monitored throughout the process. After solid separation (Whatman filter paper N°1), the supernatant pH was adjusted to 3.4 with 2 M HCl under continuous stirring to precipitate proteins (Celus et al., 2007; E. Vieira et al., 2014). This pH was mainly used as a representative value within the broader isoelectric region of BSG proteins (3.0-3.8), as previously reported in the literature (Junttila, 2022; Qazanfarzadeh et al., 2024). Precipitated protein was recovered by centrifugation (9000 rpm, 10 min, 4 °C), followed by freeze drying of the protein fraction to obtain BSG-PC. The remaining solids were washed with distilled water until neutralisation (pH 7-8) and stored for further processing.

2.4. Lignin extraction, modification and characterisation

Residual BSG solids after NTP, enzymatic hydrolysis and alkaline protein extraction (treatment 3) were used for lignin recovery (Rojas-Lema et al. (2023) with slight modifications). Briefly, BSG residue was suspended in 1.5 M NaOH at 1:10 w/v (500 mL total). The solution was heated to 140 °C for 3 h in an autoclave to facilitate lignin solubilisation, followed by liquid separation by centrifugation (12,000 rpm, 15 min, 4 °C). Sulfuric acid was gradually added to the supernatant under stirring until the pH reached 2.0, causing lignin precipitation. Precipitated lignin was separated via centrifugation (12,000 rpm, 15 min, 4 °C), freeze-dried and stored.

For the preparation of the alkaline lignin (AL), a 30 g/L lignin solution was prepared using an NaOH aqueous solution 5 M (pH 10.0). LPs were formulated according to the protocol described by Colucci et al. (2023) with some modifications. LPs were prepared by stirring 3 g of lignin in 100 mL of a 70:30 ethanol:water solution for 10 min at 500 rpm, followed by ultrasonication (Bandelin Sonorex RK 52 from Reagente 5 - Química e Electrónica Lda, Portugal) for 10 min. An aqueous phosphate-citrate buffer (pH 8) was added to the lignin solution at a rate of 14 mL/min as antisolvent using a syringe pump (KDS 200, KD Scientific, USA) for 4 min. The solution was then evaporated (R-114, Waterbath B-480, and Vacuum Controller B-721, Büchi, Switzerland) at 60 °C and 180–140 mbar, to remove the ethanol and achieve the same initial lignin concentration (30 g/L). The final lignin concentration was checked gravimetrically by drying an aliquot of the dispersion until constant weight. The LPs were characterized for particle size using a Mastersizer 3000 equipped with a Hydro MV dispersion unit (Malvern Instruments Ltd., United Kingdom), following published procedure (Colucci et al., 2023). The refractive index and absorption of the particles were set to 1.6 and 0.1, respectively. Distilled water was used as LP's dispersing media and five consecutive measurements were performed at room temperature. The number-median diameter (D50) was used for size analysis.

2.5. BC production and BNCs formulation

For BC production the bacterial strain *Komagataeibacter sucrofermentans* DSM 15973 (Leibniz-DSMZ Institute, Germany) was used and stored at −80 °C in cryovials containing 50 % (v/v) pure glycerol. A 250-mL Erlenmeyer flask was filled with 50 mLof Hestrin and Schramm medium (pH 6.0), comprising (g/L): 20.0 glucose, 5.0 peptone, 5.0 yeast extract, 2.7 disodium phosphate and 1.15 citric acid. One cryovial was inoculated into the shake flask, followed by 24-h incubation in a rotary shaker (200 rpm) at 30 °C.

BC production was done according to Efthymiou et al., 2022b. BSG hydrolysate was used as a carbon and nitrogen source. The total sugar concentration reached 20 g/L, whereas 5 g/L bacteriological peptone, 3.5 g/L yeast extract, 2.7 g/L disodium phosphate, and 1.15 g/L citric acid were added to enrich the medium. BSG hydrolysate was filter-sterilsed before fermentation using a 0.22 μm filter unit (PolycapAS, Whatman Ltd.), whereas nitrogen sources and the mineral solution were sterilized in separate (121 °C, 20 min). Batch cultures were inoculated at 10 % v/v and incubated at 30 °C for 10 days under controlled pH (5.0). At the end of the fermentation, the broth was centrifuged (9000×*g*, for 10 min, at 4 °C) and the collected BC was first washed with distilled water under boiling conditions (100 °C, three times), followed by immersion in 1 M NaOH solution for 24 h under agitation (180 rpm). BC was washed with distilled water to remove excess NaOH until reaching a pH of ~7.0, freeze-dried, ground (ECB mill, London) and stored until further use.

The modification of BC was carried out via acid hydrolysis, as reported by Sarafidou, Vlysidis, et al. (2025). More specifically, 5 g of ground BC was moistened with distilled water and homogenised for 4 min using an Ultra-Turrax T25 Basics (IKA) at 15,500 rpm. Sulfuric acid (95-97 %, Honeywell) was added to the suspension and diluted with water to reach a final concentration of 50 % (w/w) and a total volume of 50 mL. The hydrolysis process was conducted at 55 °C under continuous agitation at 500 rpm. After 48 h, distilled water (5:1 v/v) was added to terminate chemical hydrolysis, followed by 30 % hydrogen peroxide for the bleaching step. These conditions were selected based on previous structural validation under identical hydrolysis parameters (50 % H_2SO_4, 48 h, 55 °C), where controlled nanostructuring was confirmed by dynamic light scattering (~56 nm), ζ-potential (−34 mV) and X-ray diffraction analysis demonstrating preservation of cellulose I crystalline structure (crystallinity index 88.3 %) (Efthymiou et al., 2022b). In the previous work, the same protocol yielded BNC with a crystallinity index above 92 % (Sarafidou, Vlysidis, et al., 2025), further supporting the suitability of these conditions. The suspension was then maintained under continuous agitation at 200 rpm for 1 h, followed by a series of washing steps to remove excess acid. Specifically, the suspension was centrifuged three times (7500 rpm, 15 min, 4 °C), ultrasonicated at 60 kHz and 300 W for 6 min (Sonoplus 3200, Germany) and subsequently placed in dialysis bags (Medicell Membranes Ltd, 12–14 kDa). The dialysis process was performed in a water bath, with systematic water replacement until pH neutralisation was achieved. The final suspension of BNC was stored at 4 °C until further use.

2.6. Bio-based films formulation

Each BSG-RS processing strategies (Section 2.3) was studied focusing on bio-based film formulation, and the resulting film formulations are presented in Table 1. The selected strategy was further developed to produce homogeneous bio-based films.

2.6.1. Treatment 1 – films formulation after mild acid hydrolysis

After acetic acid hydrolysis, glycerol (30 % w/w, based on BSG-RS) was incorporated into the suspension, followed by heating at 80 °C until solubilisation (400 rpm, 1 h) (Merino et al., 2021). The solution was cooled down, cast into Petri dishes (90 × 15 mm), and allowed to dry for 24 h.

2.6.2. Treatment 2 – films formulation after organosolv treatment

Glycerol (30 % w/w, based on BSG-RS) was incorporated into the

Table 1
Samples nomenclature and composition resulted after the different BSG-RS processing strategies.

Treatment 1 – mild acid hydrolysis						
Name	BSG-RS (%, w/v)					Glycerol (%, w/w) [a]
T1-RS/5	5					30
T1-RS/7.5	7.5					30
T1-RS/10	10					30
Treatment 2 – organosolv treatment						
Name	BSG-RS (%, w/v)					Glycerol (%, w/w) [a]
T2-RS/70	10					30
T2-RS/80	10					30
T2-RS/90	10					30
Treatment 3 – BSG-RS fractionation						
Name	BSG-PC (%, w/v)	BNC (%, w/w) [b]	Glycerol (%, w/w) [b]	Tween-20 (%, w/v)	AL (%, w/w) [b]	LPs (%, w/w) [b]
PC/0	3.5	10	30	1	-	-
PC/5AL	3.5	10	30	1	5	-
PC/10AL	3.5	10	30	1	10	-
PC/15AL	3.5	10	30	1	15	-
PC/5LPs	3.5	10	30	1	-	5
PC/10LPs	3.5	10	30	1	-	10
PC/15LPs	3.5	10	30	1	-	15

T, treatment; RS, residual solids; BSG, brewers' spent grain; PC, protein concentrate; BNC, bacterial nanocellulose; AL, alkaline lignin; LPs, lignin particles.
[a] Based on BSG-RS.
[b] Based on BSG-PC.

black liquor, followed by continuous stirring for 1 h. Solvent casting of the resulting solution was conducted into Petri dishes (90 × 15 mm) and dried at room temperature for 24 h.

2.6.3. Treatment 3 – films formulation utilising BSG-PC

Preparation of bio-based films utilising BSG-PC was conducted following the protocol described by Efthymiou et al. (2022a), with some modifications. 3.5 % w/v BSG-PC was suspended in distilled water with the pH adjusted to 11 (2 M NaOH) under continuous stirring (300 rpm, 40 °C) for 20 min, followed by the addition of 30 % w/w glycerol, 1 % w/v tween-20 and 5 % or 10 % w/w BNC. AL and LPs were incorporated into the protein matrix in different concentrations of 5 %, 10 %, and 15 % w/w to enhance the bioactivity of the suspension. The solutions were homogenised using a rotor-stator homogenizer (CAT, Unidrive X 1000, Germany) (12,000 rpm, 5 min), followed by stirring at 80 °C for 30 min. Finally, 25 mL were poured into Petri dishes and dried at room temperature for 24 h, followed by an additional drying step at 50 °C for 24 h to ensure full water removal and film integrity. All films were stored in a desiccator prior to characterisation to allow moisture equilibrium and ensure comparable conditions among samples. The resulting films named PC/0 (without lignin), PC/5AL, PC/10AL, PC/15AL, PC/5LPs, PC/10LPs, and PC/15LPs (Table 1) were selected for further characterisation.

2.7. Characterisation of the selected films

2.7.1. Colour and UV-Vis properties

The colour of the BSG-based films was quantified by measuring the parameters L* (luminosity), a* (green-red chromaticity), and b* (blue-yellow chromaticity) using a Minolta CR-400 tri-stimulus colorimeter (Konica Minolta Sensing, Inc., Osaka, Japan). As a reference, a white background was used. The total colour difference (ΔE), colour differences (ΔC), and brown index (BI) were calculated using equations (2)–(4).

$$\Delta E = \sqrt{(L - L_0)^2 + (a - a_0)^2 + (b - b_0)^2} \quad (2)$$

$$\Delta C = \sqrt{(a - a_0)^2 + (b - b_0)^2} \quad (3)$$

$$BI = \left(\frac{(a^* + 1.75L^*)a^*}{5.645L^* + a^* - 3.012b^*} - 0.31 \right) \quad (4)$$

where L_0, a_0, and b_0 are the L, a, and b values on the film without AL and LPs incorporation (corresponding to sample PC/0).

The films were cut into pieces (1 × 4 cm), placed in a UV-vis spectrophotometer (Shimadzu UV–1900i), and the absorbance was collected within the wavelength range 200-800 nm. The absence of a sample served as the reference (blank). Transparency (T) and UV transmittance (UV%) were determined according to equations (5) and (6):

$$T = \frac{\log(\%T_{600nm})}{t} \quad (5)$$

$$UV\% = \frac{\int_{400}^{200} T(t)dt}{\int_{400}^{200} dt} \times 100 \quad (6)$$

where $\%T_{600nm}$ is the transmittance at 600 nm, and t is the film thickness (mm) measured at three different points for the film utilising a calibrated digital micrometer.

All the measurements were conducted in triplicate.

2.7.2. Antioxidant activity

The antioxidant activity of the films was determined using two different antioxidant assays. The 2,2-diphenyl-1-picrylhydrazyl (DPPH) method followed the methodology described by He et al. (2023), with some modifications. An aqueous solution of 20 mg film (10 mL working volume) was prepared and stirred for 24 h at ambient temperature. A 0.2 mM solution of DPPH in methanol was prepared. Each properly diluted sample (2 mL) was mixed with the DPPH solution (1:1 v/v) and incubated at 25 °C for 30 min in the absence of light. A control sample was prepared by replacing the sample solution with distilled water following the same procedure. The absorbance of each sample solution (A_s) and control sample (A_0) was measured at 517 nm using a UV-vis spectrophotometer (Shimadzu UV – 1900i). The DPPH radical-scavenging inhibition (%) was determined using equation (7).

$$\text{DPPH inhibition}\% = \left(\frac{A_0 - A_s}{A_0} \right) \times 100 \quad (7)$$

Additionally, the antioxidant activity was evaluated using the 2,2′-

azino-bis(3-ethylbenzothiazoline-6-sulfonic acid (ABTS) radical scavenging assay by using modified protocols described by Llana-Ruiz-Cabello et al. (2015). A stock solution of 7 mM ABTS was prepared in distilled water and mixed with 2.45 mM potassium persulfate solution at equal volumes. The mixture was incubated in the dark at room temperature for 12-16 h to generate the $ABTS^{\bullet+}$ radical cation. Prior to analysis, the $ABTS^{\bullet+}$ solution was diluted with methanol to obtain an absorbance of 0.70 ± 0.02 at 734 nm. Film extracts were prepared using the same procedure described for the DPPH assay. Then, 20 μL of sample extract was mixed with 280 μL of $ABTS^{\bullet+}$ solution, and the absorbance was measured at 734 nm after 6 min incubation using a microplate reader (Infinite M200 PRO, Tecan Group Ltd.). For the control measurement, 20 μL of methanol was used instead of the sample. All experiments were performed in triplicate. The ABTS radical scavenging activity (%) was calculated using equation (8).

$$\text{ABTS inhibition}\% = \left(\frac{A_0 - A_s}{A_0}\right) \times 100 \quad (8)$$

where A_0 and A_s correspond to the absorbance of the control and sample solutions, respectively.

2.7.3. Attenuated total reflectance Fourier transform infrared (ATR-FTIR) spectroscopy

The spectra of the raw materials and selected films were measured using an FTIR spectrometer (ABB MB3000) operating in ATR mode and equipped with Horizon MB™ FTIR software. The spectral range was analysed from 4000 to 550 cm^{-1} with 32 scans, a resolution of 4 cm^{-1} and a detector gain of 80.68.

2.7.4. Mechanical properties

The mechanical properties of the films were measured under ambient conditions using a universal testing machine (Autograph AGS-X 10 kN, Shimadzu) equipped with a 500 N load cell and pneumatic clamps. The specimens were cut (20 mm × 60 mm) and analysed with a crosshead speed of 5 mm/min at room temperature. The film thickness was determined using a calibrated digital micrometer (806.B 25, Facom), averaging three measurements at different points for each specimen. The results were presented as the average ± standard deviation.

2.7.5. Water contact angle, solubility and barrier properties

A Theta flow optical tensiometer (Biolin Scientific, Gothenburg, Sweden) was utilised to measure the water contact angle (WCA) of the films (ASTM D5946, 2017). A single distilled water drop, 4 μL in volume, was placed on three different points of the film surface and after 10 s the angle was recorder. All measurements were conducted at ambient temperature. The results were presented as the average ± standard deviation.

Water barrier properties, determined as water vapour transmission rate (WVTR) and water vapour permeability (WVP), were assessed using the modified method outlined by Athanasopoulou et al. (2025). Films were cut (2 × 2 cm^2), placed on the top of glass vials containing 4 g silica gel (0 % relative humidity), sealed and stored in a desiccator at 25 °C filled with $BaCl_2$ (90 % relative humidity). The weight gain of the vials was recorded every 2 days over 3 weeks. The WVTR ($g/(s \times m^2)$) and WVP ($g/(m \times Pa \times s)$) were calculated according to equations (9) and (10), respectively.

$$WVTR = \frac{\Delta W}{\Delta t} \times A \quad (9)$$

$$WVP = \frac{WVTR \times d}{\Delta P} \quad (10)$$

where ΔW/Δt (g/day) is the weight gain of the vials per day; A (m^2), the exposed surface of the film; d (mm), the average thickness of the film; ΔP (kPa), the vapour pressure difference between the two sides of the films. The results were expressed as the average of five replicates.

The water solubility of films was determined by the modified method reported by Athanasopoulou et al. (2025). Films were cut (2 × 2 cm^2), weighed (W_1) and placed into an oven to dry (80 °C) for 24 h. The dried films were cooled, weighed (W_2) and immersed in 50 mL of distilled water. After 24 h, the swollen films were dried (80 °C) for 24 h and re-weighed (W_3). The water solubility was calculated according to equation (11).

$$\textit{Water solubility}(\%) = \frac{(W_2 - W_3)}{W_2} \times 100 \quad (11)$$

All measurements were performed in triplicate for each film sample.

2.7.6. Scanning electron microscopy (SEM)

SEM analysis of the selected bio-based films (PC/0, PC/5AL, and PC/5LPs) was conducted using a scanning electron microscope JEOL JSM-6010LV using secondary electron mode. The system is equipped with an INCAx-Act PentaFET Precision energy-dispersive X-ray spectrometer (EDS; Oxford Instrument, UK). Prior to imaging, the films were fractured in liquid nitrogen to obtain brittle cross-sections, mounted on aluminium stubs, and coated with a 1.5 nm layer of Pt. The samples were then transferred into the SEM chamber and analysed vertically for cross-sections and horizontally for surface views.

2.7.7. Thermogravimetric analysis

The thermal stability of the selected films was determined by thermal decomposition (TG) and derived thermogravimetry (DTG) curves. The analysis was performed on a TG model 20F3 Tarsus device (Selb, Germany), using approximately 7 mg of sample packed in aluminum crucibles. Heating was conducted from 30 °C to 800 °C at a rate of 10 °C/min in an inert nitrogen atmosphere. The thermograms obtained were processed using Netzsch Proteus Thermal Analysis software (version 5.2.1).

2.7.8. X-ray diffraction (XRD)

XRD analysis was performed to determine the crystalline phases of the selected samples. Measurements were carried out using a Bragg-Brentano diffractometer equipped with CuKα radiation operated at 40 kV and 40 mA. Diffractograms were collected over a 2θ range of 5-70° with a step size of 0.04° s^{-1}. Phase identification and crystallinity (%) were determined using the Bruker's DIFFRAC.EVA software in combination with the Crystallography Open Database, where the crystallinity (%) was estimated using the ratio between the area of the peaks and the total area of the diffractogram.

2.8. Application of films on salmon fillets

Salmon fillets (*Salmo salar*) supplied from the local market were immediately transferred to Laboratory of Food Process Engineering (Agricultural University of Athens), treated, and packed under aseptic conditions. More specifically, salmon fillets were cut into slices (3 × 3 × 3 cm, average weight 20 ± 2 g), placed into plastic cups (50 mL volume and 4 cm diameter), sealed with PVC, PC/0, PC/5AL, or PC/5LPs and stored at 4 °C (Sanyo MIR 153, Sanyo Electric, Ora-Gun, Japan) for 9 days. The packaging materials were disinfected under UV radiation for 20 min, prior to the assay. Sampling was performed daily from day 1 to day 4, with an additional measurement on day 9 to assess the later-stage microbial development.

2.8.1. Microbiological analysis

For each sampling time, 10 g of each sample was transferred into sterile Blender Bags (BagLight® 400 mL, Interscience) under aseptic conditions. Sterile Ringer's solution (Condalab) was added to achieve a 1:10 w/v ratio, and the diluted samples were homogenised for 1 min using a stomacher (BagMixer 400 P, Interscience). Appropriate serial

decimal dilutions in Ringer's solution were prepared, followed by plating. The enumeration of total aerobic mesophilic counts (TMC) was conducted using Tryptic Glucose Yeast Agar (PCA), whereas for *Pseudomonas* spp. and Enterobacteriaceae, Pseudomonas Agar Base with the addition of CFC (Cetrimide, Fucidine, Cephalosporine) supplement and Violet Red Bile Glucose Agar (VRBG) (Condalab) were used, respectively. Incubation for both TMC and *Pseudomonas* spp. was conducted at 25 °C for 48 h, whereas for Enterobacteriaceae was conducted at 37 °C for 24 h. During Enterobacteriaceae enumeration, only red-purple colonies displaying biliary precipitate were measured.

The Baranyi growth model (Baranyi & Roberts, 1995) was used for microbial growth kinetics modelling, using the software DMFit (IFR, Institute of Food Research, Reading, UK) for curve fitting (http://www.combase.cc/index.php/en/).

2.8.2. Sensory analysis

The sensory properties of salmon fillets were anonymously evaluated by a panel of six trained adult assessors, properly instructed in the identification of spoilage characteristics in fish fillets (Botta, 1996), all of whom volunteered. Appropriate forms were prepared using descriptive terms for each sensory parameter (colour, odour and overall impression), with each sensory parameter scored separately on a 1–9 descriptive scale (1 = lowest quality, 9 = highest quality and 5 = limit of acceptability) (Tsironi & Taoukis, 2017). Before involvement in the study, each person gave informed written consent. Participants were also free to withdraw their consent at any point without needing to provide a reason. No additional ethical approval was necessary. All relevant procedures were followed to ensure participants' rights and privacy.

2.9. Statistical analysis

A one-way analysis of variance on BSG-based films properties and shelf-life test of salmon fillets was carried out, followed by a posthoc analysis (Duncan's multiple range test) using STATGRAPHICS Centurion 293 XVII (Version 17.2.00).

2.10. Analytical methods

Initial moisture was determined by subjecting 2 g of wet BSG in crucible to drying (105 °C) for 24 h. At the same time, ash content was determined by heating the samples in a muffle furnace at 575 °C until incineration (Sluiter et al., 2008a).

Dextrin quantification, expressed as glucan equivalents, was accessed as reported by Argeiti et al. (2024). BSG aqueous suspension (1:10 w/v) was prepared and subjected into 40 °C under continuous agitation on a hot plate stirrer (Witeg Labortechnik GmbH, Germany) for 4 h. Liquid was separated via centrifugation (9000 rpm, 4 °C, 10 min), followed by the addition of 1 mL commercial glucoamylase (10 U enzymatic activity) and incubation in a water bath (50 °C for 7 h).

Glucan, xylan, arabinan, galactan, mannan and lignin contents were carried out after the removal of soluble components (Sluiter et al., 2008c), followed by a two-step hydrolysis process by H_2SO_4 (Sluiter et al., 2008b).

Glucose, xylose, arabinose, galactose and mannose concentrations were determined using High-Performance Liquid Chromatography (HPLC) (Shimadzu UFLC XR system, Japan). The HPLC system was equipped with a Phenomenex Rezex ROA-Organic acid H^+ column (300 mm × 7.8 mm) and a refractive index detector (Shimadzu, Japan). The column was set at 65 °C for the analysis, and a 10 mM H_2SO_4 aqueous solution was used as the mobile phase for the elution step (flow rate of 0.6 mL/min). Prior to analysis, the samples were properly diluted and filtered using a PTFE membrane (0.22 μm). Standard curves were developed using commercial sugars.

Protein content was determined by the Kjeldahl method using a Tecator digester and a distillation unit (Foss Tecator Kjeltec 8200 Auto Distillation Unitand) applying a Nitrogen-Protein Factor of 6.25. Lipid content was quantified by subjecting BSG in a Soxhlet apparatus for 6 h using hexane.

BSG phenolic-rich extract was obtained by suspending BSG (1:20 w/v) in 70% ethanol acidified with 0.1 % v/v HCl (0.1 M). The extract was ultrasonicated (20 min) and filtered for the separation of the extract. The filtrate was vacuum-evaporated to remove ethanol and then rediluted with 10 mL of analytical-grade methanol. Total phenolic content (TPC) of BSG antioxidant-rich extract was measured using the Folin-Ciocalteu colourimetric method and identified as mg of gallic acid equivalents (GAE) per g BSG (Filippi et al., 2021).

3. Results and discussion

3.1. Compositional analysis of brewers' spent grain

The composition of BSG (% dry basis) is presented in Table 2. Moisture was 68.5 %, within a typical range of 66-85 % (Argeiti et al., 2024; Santos et al., 2024). BSG can be described as a lignocellulosic material, rich in cellulose, hemicellulose and lignin (Ikram et al., 2017), accounting for almost 50 % of dry biomass (Table 2). The holocellulose fraction was 38.9 %, mainly in the form of glucan (17.2 %), xylan (15.4 %), and arabinan (4.8 %), followed by galactan (1.3 %) and mannan (0.3 %). Protein and lignin contents were 20.5 % and 9.6 %, respectively, while lipids, ash and phenolic compounds accounted for 6.3 %, 2.4 % and 0.5 % GAE, respectively. BSG composition depends on the raw materials, the beer production process and the additives used during mashing (Lynch et al., 2016). During brewing, starch is saccharified to maltose, maltotriose, and dextrins (Lynch et al., 2016). In the present study, those fractions were defined as dextrin, expressed as glucan equivalents equal to 21.3 %. BSG protein composition is influenced by both the beer production process and raw materials, ranging from 14.3 % to 24.3 % (Carvalheiro, 2004; Pinheiro et al., 2019). In contrast, BSG lignin composition is primarily affected by the raw material, with values ranging from 8.9 % to 19.4 % (Meneses et al., 2013; Pinheiro et al., 2019; Rojas-Chamorro et al., 2020).

Proteins in BSG are surrounded by the cell wall, composed of arabinoxylans and lignin attached to the cellulose fibrils (Qin et al., 2018), limiting solvent accessibility. Protein recovery requires cell wall

Table 2
Composition of the brewers' spent grain in this study and comparison with compositions found in literature.

Composition (%, dry basis)	This study	Literature	Reference
Moisture	68.5 ± 0.1	66.0-85.0	(Argeiti et al., 2024; Santos et al., 2024)
Dextrin[a]	21.3 ± 0.1	15.9	Argeiti et al. (2024)
Glucan	17.0 ± 1.0	15.2 – 20.6	(Qin et al., 2018; Rojas-Chamorro et al., 2020)
Hemicellulose	21.8 ± 0.7	19.3 – 41.9	(Argeiti et al., 2024; Carvalheiro, 2004; Meneses et al., 2013; Pedro Silva et al., 2004; Pinheiro et al., 2019; Qin et al., 2018; Rojas-Chamorro et al., 2020)
Xylan	15.4 ± 0.3	7.0 – 20.6	
Arabinan	4.8 ± 0.3	2.6 – 6.8	
Galactan	1.3 ± 0.1	1.3 – 3.7	
Mannan	0.3 ± 0.02	0.3 – 1.1	
Protein	20.5 ± 0.3	14.3 – 24.6	(Carvalheiro, 2004; Pinheiro et al., 2019)
Lignin	9.6 ± 0.2	8.9 – 19.4	(Meneses et al., 2013; Pinheiro et al., 2019; Rojas-Chamorro et al., 2020)
Soluble	1.4 ± 0.01	1.9 – 5.5	
Insoluble	8.3 ± 0.2	6.7 – 17.5	
Lipids	6.3 ± 0.7	3.7 – 11.0	(Argeiti et al., 2024; Ikram et al., 2017)
Ash	2.4 ± 0.3	1.2 – 4.6	(Carvalheiro, 2004; Mussatto & Roberto, 2006)
Total phenolic content[b]	0.5 ± 0.03	0.1 – 2.0	(Lynch et al., 2016; Socaci et al., 2018)

[a] Expressed as glucan equivalents.
[b] Expressed as gallic acid equivalents.

degradation, leading to structural carbohydrate losses (Junttila, 2022). An efficient biorefinery targets dextrins and holocellulose recovery before protein separation, to minimise sugar losses. In this context, NTP pre-treatment followed by enzymatic hydrolysis has been suggested to maximise sugar release while preserving minimal losses of protein and lignin fractions (Argeiti et al., 2024).

3.2. Plasma treatment and enzymatic hydrolysis

Fig. 1 presents the process flow diagram proposed in this study. After NTP pre-treatment, BSG contained mainly 28.5 % glucan, 29.1 % hemicellulose, 22.4 % protein and 10.1 % lignin. Approximately 80 % of dextrins were solubilised into plasma liquid, together with protein (13 %). These findings agree with reports that plasma-generated reactive species promote lignin depolymerisation and protein migration to the aqueous phase (Devnani et al., 2023; Filippi et al., 2025; Perrocheau et al., 2005). Enzymatic hydrolysis of pre-treated BSG leads to a sugar-rich hydrolysate composed mainly of glucose (74.3 %) and xylose (14.5 %), followed by arabinose (8.1 %), galactose (2.3 %) and mannose (0.8 %). The hydrolysate was subsequently utilised for BC production through microbial fermentation (Section 2.5.).

3.3. Evaluation of bio-based films formulation utilising BSG-RS solids

The utilisation of BSG-RS for the formulation of bio-based films was assessed by testing three different treatments (Fig. 2). Mild acid hydrolysis (treatment 1), a conventional pre-treatment for lignocellulosic biomass, resulted in insoluble residues and a rough surface, even at the lowest solids concentration (5 % w/v). This outcome is consistent with previous reports showing that mild acid conditions are ineffective for lignocellulose substrates, as the lignin content of BSG-RS (16.0 %) contributes to its recalcitrant structure, rendering this method unsuitable for further analysis (Puligundla & Mok, 2021). Organosolv treatment (treatment 2), a method often used to improve lignin solubilisation, produced films with a smooth surface (De Sousa Nascimento et al., 2021). However, the films exhibited a dark colour and a persistent acetic acid odour limiting their suitability as a primary film-forming matrix and restricting their potential use to an additive role (R. M. Vieira et al., 2025; Zolfaghari et al., 2024).

To further optimise the solubilisation of BSG-RS, protein- and lignin-rich fractions were recovered and utilised as matrices for bio-based films formulation (treatment 3). Protein extraction of BSG is challenging due to the strong association between proteins and lignin within the substrate (Qin et al., 2018). The recovered protein-rich fraction (BSG-PC) exhibited a protein purity of 52.8 %, as well as lignin and ash contents of

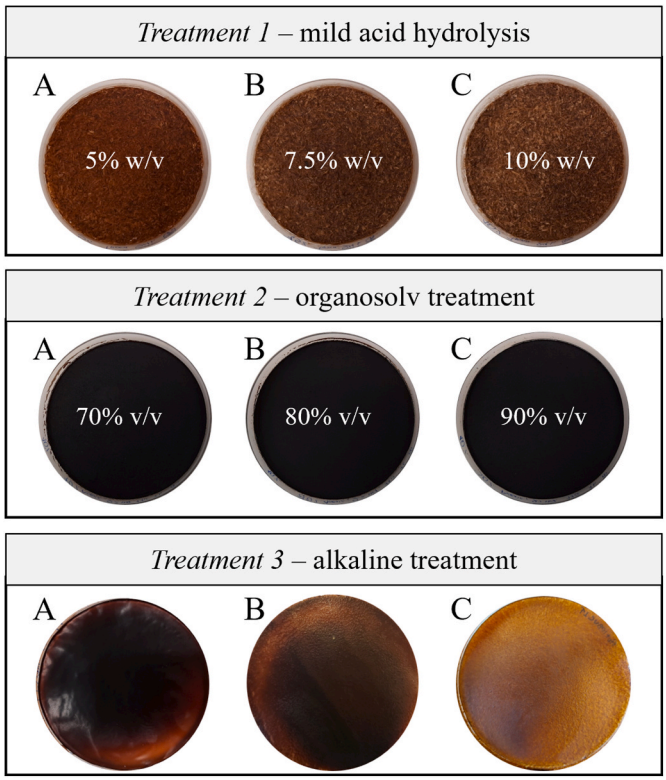

Fig. 2. Films formulations from different treatments of residual solids of brewers' spent grain (BSG-RS). *Treatment 1* – mild acid hydrolysis with initial concentrations of (A) 5 % w/v, (B) 7.5 % w/v, and (C) 10 % w/v; *Treatment 2* – organosolv treatment using (A) 70 % v/v, (B) 80 % v/v, and (C) 90 % v/v acetic acid solution; *Treatment 3* – alkaline treatment with 3.5 % w/v protein concentrate from brewers' spent grain (BSG-PC), 30 % glycerol, 1 % tween 20; (A) without bacterial nanocellulose (BNC), (B) 5 % w/w BNC, and (C) 10 % w/w BNC.

36.6 % and 9.8 %, respectively. These results are in accordance with another study that recovered a protein-rich fraction via alkaline treatment directly from BSG (Qazanfarzadeh et al., 2024).

BSG-PC was used as the raw material to produce bio-based films without a plasticiser, resulting in a rigid, brittle structure. The incorporation of a plasticiser reduces protein-protein interactions, thereby improving film flexibility and dispersibility (Calva-Estrada et al., 2019). The incorporation of 30 % glycerol (w/w, protein-basis) led to a more

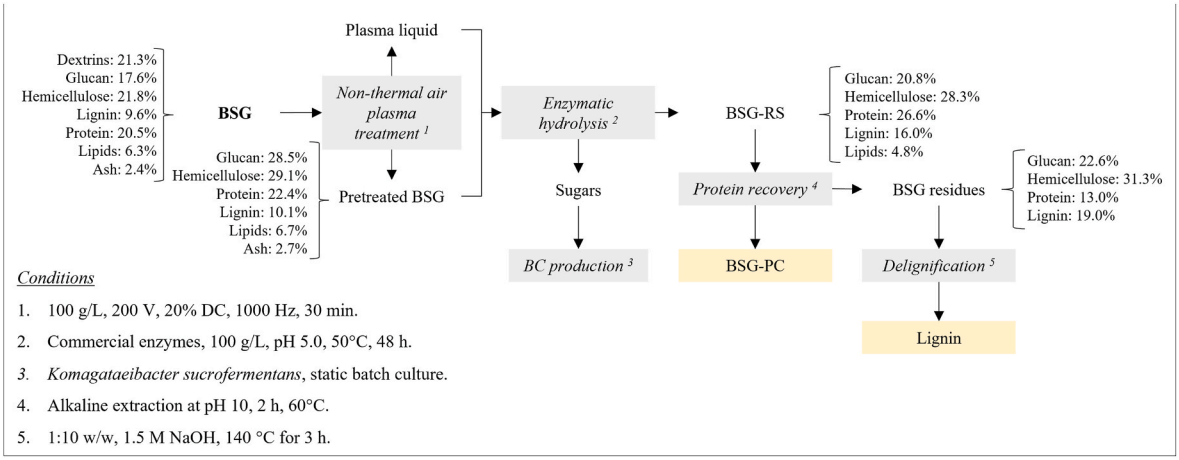

Fig. 1. Biorefinery development of brewers' spent grain (BSG) following the selection of Treatment 3 for BSG-based packaging film formulation. RS, residual solids; PC, protein concentrate; BC, bacterial cellulose.

uniform material, though it remained brittle and dark (Fig. 1, treatment 3A). To further improve structural properties, BNC was incorporated as a reinforcing agent at 5 % and 10 % (w/w, protein-basis), based on previous studies reporting enhanced mechanical strength in bio-based films (Efthymiou et al., 2022a; Sarafidou, Tsouko, et al., 2025). Incorporation of 5 % BNC resulted in visually lighter, more uniform films, while higher BNC levels further reduced their dark colour, possibly due to improved polymer dispersion.

It is to highlight that the presence of lignin in the BSG-PC not only enhances the bioactivity of the bio-based films, as reported by Qazanfarzadeh et al. (2024) playing an important role in improving the films' functional properties, but also contributes to the full valorisation of all BSG fractions. For this reason, the selected formulation (Fig. 2, treatment 3C) was further developed by incorporating the lignin-rich fraction extracted from the remaining BSG residues after BSG-PC recovery. This fraction exhibited a lignin purity of 64.9 %, and protein and ash contents of 22.1 % and 10.2 %, respectively. Lignin valorisation as a functional and reinforcing agent into bio-based films was explored using two forms (AL and LPs), enabling identification of the lignin type most suitable for enhancing the bioactivity of the active film formulations. After the lignin-rich fraction modification step, the formulated LPs had an average diameter of 746 ± 2 nm.

3.4. Characterisation of bio-based films

3.4.1. Films appearance and UV-shielding properties

All formulated BSG-based films exhibited a dark brown colour, as presented in Fig. 3A. Table 3 shows the colour parameters (L*, a*, and b*), colour change (ΔE, ΔC) and the browning index (BI) values of the bio-based films produced from BSG-PC and crude lignin fraction. The dark colour was primarily attributed to the BSG-PC matrix's intrinsic brown colour. Still, significant impact of the film's colour was observed when lignin was incorporated. The presence of chromophore groups in BSG-PC, due to its lignin content, also contributes to the film's dark appearance (Y. Zhang & Naebe, 2021). Similar brown colour of BSG-based films have been reported in the literature (Oztuna Taner et al., 2023; Proaño et al., 2020; Shroti & Saini, 2022).

Regarding the appearance of the lignin-loaded films, there was no clear trend regarding the colour parameters with increased lignin addition (Table 3). In the case of AL, lightness (L*) was affected, with slight differences between the studied AL concentrations (ranging between 22.77 and 25.45). A similar trend was observed for the redness (a*) and yellowness (b*) of the AL-loaded films (9.89 to 13.16 and 4.43 to 6.28, respectively). ΔE and BI values of PC/15AL were slightly lower compared to PC/5AL, without significant differences (*p-value* < *0.05*), whereas 10 % AL addition led to ΔE increasing (2.84) and BI decreasing (5.63) (*p-value* > *0.05*). A similar trend was observed with ΔC values, with significant alterations between the different AL concentrations (1.32-2.41) (*p-value* < *0.05*). The incorporation of LPs into the matrix led to a decreasing trend in L*, with PC/15LPs showing the lowest value of 20.48. Modifications on a* and b* were also observed (ranged between 7.27 to 13.50 and 3.59 to 6.63), without a clear trend on higher LPs concentrations (*p-value* < *0.05*). The colour changes affected the ΔE, ΔC and BI values of the bio-based films, ranging from 2.65 to 5.11, 2.39 to 5.11 and 3.88 to 8.18, respectively.

Colour changes have been previously observed in bio-based films with the addition of different lignin concentrations (Rojas-Lema et al., 2023; R. M. Vieira et al., 2025). Colour modification in lignin-loaded films at higher concentrations is likely linked to the intrinsic dark colour of lignin and the increased overall lignin content in the matrix. In LPs-containing films, some particle clustering is visible at elevated loadings (Fig. 3A), which can locally intensify colour, but this effect appears only when the concentration is sufficiently high. Similar concentration-dependent darkening has been reported in other

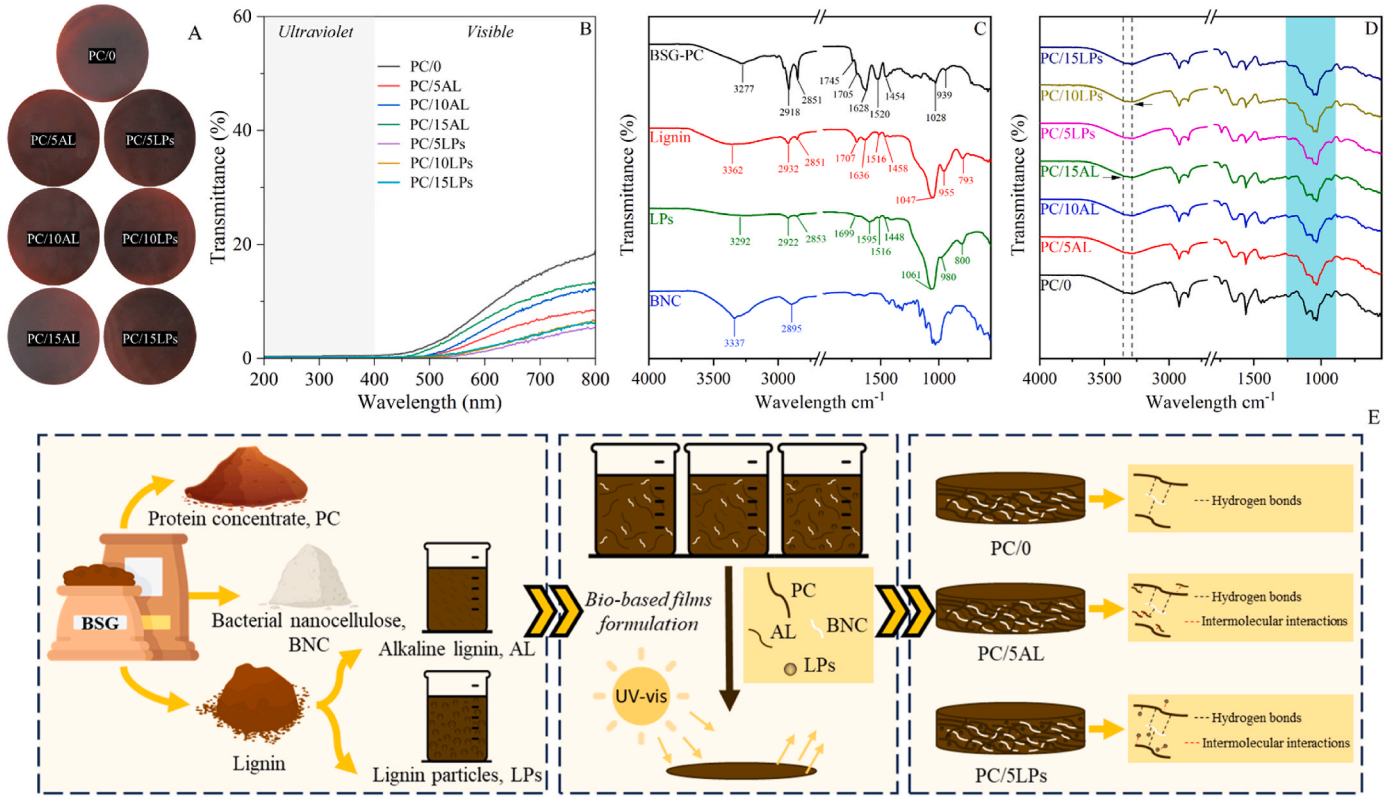

Fig. 3. A. Films appearance, B. UV-vis transmittance spectra, C. ATR-FTIR spectra of raw materials, D. ATR-FTIR spectra of brewers' spent grain (BSG)-based films, and E. Selected strategy for BSG-based films and proposed interactions between their components on the selected formulations (PC/0, PC/5AL and PC/5LPs). PC; protein concentrate; AL, alkaline lignin; LPs, lignin particles.

Table 3
Colour parameters, optical properties and antioxidant activities of the bio-based films from brewers' spent grain.

Film	L*	a*	b*	ΔE	ΔC	BI	Transparency	DPPH inhibition%	ABTS inhibition%
PC/0	24.27 ± 0.32^{c}	12.29 ± 0.40^{d}	4.57 ± 0.04^{b}	-	-	7.11 ± 0.26^{d}	5.11 ± 0.12^{d}	39.79 ± 0.49^{a}	38.20 ± 1.00^{a}
PC/5AL	24.13 ± 0.03^{c}	12.99 ± 0.28^{e}	6.28 ± 0.17^{d}	1.86 ± 0.25^{a}	1.86 ± 0.25^{b}	7.88 ± 0.22^{ef}	3.17 ± 0.40^{c}	40.00 ± 4.82^{a}	41.03 ± 2.73^{a}
PC/10AL	22.77 ± 0.13^{b}	9.89 ± 0.15^{c}	4.43 ± 0.07^{b}	2.84 ± 0.10^{b}	2.41 ± 0.15^{c}	5.63 ± 0.11^{c}	3.63 ± 0.57^{c}	43.29 ± 1.23^{abc}	44.93 ± 1.00^{b}
PC/15AL	25.45 ± 0.14^{d}	13.16 ± 0.17^{ef}	5.56 ± 0.16^{c}	1.77 ± 0.26^{a}	1.32 ± 0.23^{a}	7.76 ± 0.13^{e}	4.78 ± 0.21^{d}	44.66 ± 0.01^{bc}	45.26 ± 0.99^{b}
PC/5LPs	25.42 ± 0.35^{d}	13.50 ± 0.32^{f}	6.63 ± 0.27^{e}	2.65 ± 0.49^{b}	2.39 ± 0.39^{c}	8.18 ± 0.24^{f}	0.41 ± 0.68^{a}	47.22 ± 049^{c}	46.32 ± 1.45^{b}
PC/10LPs	24.54 ± 0.32^{c}	7.27 ± 0.21^{a}	3.59 ± 0.16^{a}	5.12 ± 0.22^{c}	5.11 ± 0.21^{e}	3.88 ± 0.13^{a}	1.26 ± 0.57^{b}	45.65 ± 0.41^{bc}	45.12 ± 0.71^{b}
PC/15LPs	20.48 ± 031^{a}	8.27 ± 0.13^{b}	4.55 ± 0.11^{b}	5.53 ± 0.28^{c}	4.02 ± 0.13^{d}	4.74 ± 0.08^{b}	1.52 ± 0.40^{b}	41.36 ± 0.74^{ab}	45.59 ± 0.91^{b}

Statistically significant differences are illustrated by means followed by different letters in the same column (p-value < 0.05). PC, protein concentrate; AL, alkaline lignin; LPs, lignin particles.

lignin-based biopolymer films (L. Silva et al., 2024; W. Zhang et al., 2022).

Light transmission spectra at selected wavelength range (200-800 nm) and transparency values of the BSG-PC-based films are presented in Fig. 3B and Table 3, respectively. Whereas transparency is a favourable characteristic of food packaging materials, it is associated with low UV barriers and, thus, reduced food protection against oxidative deterioration (Basbasan et al., 2022; X. Li et al., 2025). In the present study, all the formulations present strong UV-shielding properties (≤0.6 % UV transmittance) (Fig. 3B) and low transparency values (Table 3). PC/0 showed a transparency of 5.11 %. The incorporation of AL reduced the transparency by up to 38 %, whereas the addition of LPs further reduces the transparency (up to 92 %), with final values ranging from 0.41 % to 1.52 %. These results align with previous reports demonstrating that lignin acts as an effective reinforcing agent in bio-based films, contributing UV-shielding properties (Wang et al., 2021).

3.4.2. Antioxidant properties

The antioxidant activity of the bio-based films (0.5 g/L film solution) is presented in Table 3, determined by their ability to scavenge DPPH and ABTS radicals (DPPH and ABTS inhibition%). PC/0 demonstrated a strong DPPH inhibition of 39.79 %, probably due to the presence of chromophore groups on the BSG-PC, such as phenolic and ketone (Zhang & Naebe, 2021). Addition of 5 % and 10 % AL increased DPPH inhibition to 43.29 %, without significant differences (p-value > 0.05). Further AL addition (15 %) slightly decreased the DPPH inhibition (41.36 %), without significant differences with PC/10LPs (p-value < 0.05). Comparing the 5 % addition of lignin using the different forms, PC/5LPs have significantly higher antioxidant activity (47.22 %) compared to PC/5AL (40.00 %) (p-value < 0.05).

In the ABTS assay, the control film (PC/0) exhibited an ABTS inhibition of 38.20 %. Incorporation of AL increased the radical scavenging activity, reaching 44.93 % and 45.26 % for PC/10AL and PC/15AL, respectively, which were significantly higher than PC/0 and PC/5AL (p-value < 0.05). Films containing LPs also showed enhanced ABTS inhibition. PC/5LPs presented the highest antioxidant activity (46.32 %), while PC/10LPs and PC/15LPs exhibited similar inhibition values (45.12 % and 45.59 %, respectively), without significant differences among them (p-value > 0.05). Overall, the ABTS results follow a similar trend to the DPPH assay, confirming that the incorporation of lignin improves the radical scavenging capacity of the films.

Overall, the presence of functional groups such as phenolic hydroxyl groups affects lignin's antioxidant activity. In contrast, lignin's physical morphology also affects the surface area available for reaction during analysis (L. Silva et al., 2024). In this regard, the modification of BSG lignin to particles induces a molecular rearrangement, in which hydrophilic OH groups are oriented toward the particle surface, accompanied by a reduction in lignin size. This modification increases the accessibility of functional groups, thereby enhancing antioxidant and UV-shielding performance of lignin (Österberg et al., 2020; Zhang et al., 2019), which explains the higher antioxidant activity observed for PC/5LPs compared to PC/5AL.

3.4.3. Structural characterization of BSG-based films

The ATR-FTIR spectra of raw materials (BSG-PC, lignin, LPs and BNC) and BSG-based films between 4000 and 550 cm^{-1} are presented in Fig. 3C and D. Across all the samples, the transmittance band between 3600 cm^{-1} and 3000 cm^{-1} is characteristic of the O−H and N−H stretching vibration, whereas the peaks between 2932 and 2851 cm^{-1}, represent the C−H stretching vibrations of the molecules (Jaguey-Hernández et al., 2023; Qazanfarzadeh et al., 2024; Rojas-Lema et al., 2023). The peaks around 1028 cm^{-1} and 939 cm^{-1} on BSG-PC are associated with the C–O vibrations and β-glycosidic bonds of the residual sugars on the molecule. Other main peaks of BSG-PC are located at 1628 cm^{-1}, and between 1520 cm^{-1} and 1454 cm^{-1}, characteristic of C=O stretching vibration on amide I, and N−H bending/C−N stretching vibrations on amide II, respectively (Qazanfarzadeh et al., 2024; Rojas--Lema et al., 2023). These peaks are almost absent in the lignin spectrum, being in line with the low protein content of that fraction.

Fig. 3C shows that lignin and LPs presented similar spectral features, indicating similar structures. However, the formation of new hydrogen bonds on LPs, as compared with lignin, was observed, evidenced by a shift of the -OH peak from 3362 cm^{-1} to 3292 cm^{-1} (He et al., 2019). The peaks between 1636 and 1448 cm^{-1} are attributed to C=C skeletal vibrations, confirming the presence of aromatic rings (L. Silva et al., 2024; Zolfaghari et al., 2024). Additional shifts in the lignin peaks at 2932 cm^{-1}, 1707 cm^{-1} and 1635 cm^{-1} toward lower wavelengths (2922 cm^{-1}, 1699 cm^{-1} and 1595 cm^{-1}, respectively), corresponding to structural alterations between the C-H, C=O and C-N groups. Moreover, the shift of the peaks at 1047 cm^{-1} and 955 cm^{-1} to higher wavelengths (1061 cm^{-1} and 980 cm^{-1}, respectively) indicates structural changes in C−O−C groups (Qazanfarzadeh et al., 2024). These spectral changes further confirm that the modification process induces a reorientation of lignin molecules, exposing hydrophilic -OH groups at the particles surface while retaining hydrophobic groups within the particle core.

The potential interactions between BSG-PC and lignin on the BSG-based films were investigated in Fig. 3D. The characteristic bands of BNC at ~1630 cm^{-1} and 1428 cm^{-1} (C=O stretching and C–H bending vibrations) overlapped with the film matrix signals, making challenging the identification of their interactions. However, the shift of the -OH peak on PC/0 (from 3277 cm^{-1} to 3286 cm^{-1}) compared to BSG-PC are related to hydrogen bonds formulated between the polymers (Rojas-Lema et al., 2023; Sarafidou, Forys, et al., 2025). The shift of the peak from 1109 cm^{-1} in PC/0 to 1101 cm^{-1} in the lignin-reinforced films indicates the formation of intramolecular interactions between BSG-PC and lignin. Similar intramolecular interactions between lignin and protein have been previously reported by Rojas-Lema et al. (2023). Increasing the concentration of AL in the film matrix further influenced the hydrogen bonds interaction, as reflected by the shift of the -OH peak from 3342 cm^{-1} to 3329 cm^{-1}, a change probably associated with lignin aggregation and the formation of more compact microdomains within the matrix (Shroti & Saini, 2022). In the case of LPs incorporation, a shift of the peak from 1246 cm^{-1} up to 1232 cm^{-1} was observed (C=O stretching vibrations), indicating interactions involving the acetyl group of lignin (Qazanfarzadeh et al., 2024). This behaviour is in line with the

structural reorientation during LPs formation, which exposes polar acetyl groups at the particle surface, enabling them to participate in hydrogen bonding with functional groups in the protein matrix. All these spectral modifications demonstrate that both AL and LPs interact with BSG-PC through hydrogen bonding and other interactions, with their nature and extent depending on the lignin type and concentration.

3.4.4. Water interaction and barrier properties

Water barrier properties, surface hydrophobicity and wettability are closely linked to the final application of the films as food packaging materials. The water interaction properties of the bio-based films are presented in Table 4. PC/0 showed high water solubility (88.2 %) and WVP (1.35×10^{-8} g/s m Pa), indicating the hydrophilic nature of the films. Similar WVP and water solubility values were reported on BSG-based films, ranging between 0.21×10^{-10} to 84.9×10^{-10} g/s m Pa and 43.05 % to 89.78 %, respectively (Proaño et al., 2020; Qazanfarzadeh et al., 2024). WCA of PC/0 was 28.90° (<90°), further enhancing the hydrophilic behaviour of BSG-PC. Incorporation of AL led to water solubility up to 91.8 %, without significant differences among the different AL concentrations (*p-value* > *0.05*). A similar trend was observed in WVP values, with PC/0, PC/5AL, and PC/10AL showing no difference, whereas further AL addition led to a slight increase in WVP (2.15×10^{-8} g/s m Pa). This increase is probably associated with lignin aggregation within the film matrix, which can generate larger void space (Shroti & Saini, 2022). These observations are in line with the FTIR results, which indicate modifications in hydrogen bonding in the PC/15AL formulation. However, a WCA increase up to 39.00° was observed with the addition of high AL concentrations (10 % and 15 % AL), probably due to the hydrophobic nature of lignin. The formation of hydrogen bonds between BSG-PC and AL increased the WCA, as there is no excess of unbonded hydroxyl groups available for intermolecular interactions (Priyadarshi et al., 2021; Rojas-Lema et al., 2023). A similar trend on WVP and WCA was observed on the study of Silva et al. (2023), who investigated the effect of kraft lignin incorporation (2 %, 4 %, 6 %, and 8 % w/w, protein-basis) into whey protein isolate films.

Incorporation of LPs modified the water solubility of the films (*p-value* < *0.05*), without significant differences among PC/5LPs, PC/10LPs and PC/15LPs (*p-value* > *0.05*). WVP values showed an increasing trend with LPs addition, with no significant difference with the blank sample (PC/0) (*p-value* > *0.05*). The slight increase observed at 15 % LPs incorporation is probably related to excess lignin within the matrix, where LPs agglomeration reduces film cohesiveness, facilitating the water vapour diffusion within the matrix (Rojas-Lema et al., 2023). WCA values decreased significantly when high LPs concentrations were used, highlighting the hydrophilic nature of LPs. This behaviour is in line with the FTIR results, which indicate exposure of polar functional groups, such as acetyl-related C=O groups, at the LPs surface. Their presence, combined with LPs agglomeration, creates irregularities on the film surface, resulting in lower WCA values (K. F. Silva et al., 2023). Thus, AL and LPs incorporation at low concentrations (PC/5AL, PC/10AL and PC/5LP) probably act as a binder, forming a compact network, whereas further addition reduces the interactions with the matrix and makes the film more hydrophilic.

3.4.5. Mechanical properties

The mechanical properties of the bio-based films, including tensile strength, Young's modulus, and elongation at break, are shown in Table 4. The control film (PC/0) exhibited a tensile strength of 2.3 MPa, an elongation at break of 3.9 %, and a Young's modulus of 173.9 MPa. Films rigidity was enhanced by the addition of AL or LPs, as tensile strength was reduced up to 52.2 %, with unsignificant differences between PC/0 and PC/15AL (*p-value* > *0.05*). Even at the highest AL concentration (PC/15AL), the elongation at break was significantly lower than the control film (PC/0). A different trend was observed upon incorporating LPs into the BSG-PC matrix. Notably, PC/5LPs showed a significant increase in elongation at break to 4.8 %, representing a 23 % improvement (*p-value* < *0.05*), and indicated enhanced film elasticity. This increase was followed by a decreasing trend at higher LPs concentrations of 1.9 % (PC/10LPs) and 0.6 % (PC/15LPs). This decline is in align with the previous findings (Sections 3.4.3. and 3.4.4.), where excessive LPs concentration in the matrix was related to the formation of agglomerates, resulting in a higher number and size of pores (Rojas-Lema et al., 2023)

The highest Young's modulus value was observed on PC/5AL of 412.5 MPa, highlighting the rigidity of the sample. Further AL addition decreased Young's modulus, with PC/15AL having no significant difference with the control sample (PC/0). LPs addition increased Young's modulus, which ranged between 92.3 and 188 MPa, with PC/10LPs and PC/15LPs showing no differences with the control (PC/0). Mechanical properties are similar to those of other studies utilising lignin-rich biomass (Merino et al., 2021; Moreirinha et al., 2020). Ineffective incorporation of lignin into polymer matrices resulted in particle agglomeration or phase separation due to poor interfacial bonding between the matrix and the filler (Zhang & Naebe, 2021). This interpretation is consistent with the findings from the water interaction properties, where increasing LPs incorporation led to higher WVP values (Section 3.4.4.).

Based on the combined physicochemical, barrier, and mechanical results, PC/0, PC/5AL, and PC/5LPs were selected for further evaluation. PC/0 served as the reference material, whereas PC/5AL represented the best-performed AL-reinforced formulation, exhibiting the highest stiffness (Young's modulus) without excessive loss of flexibility or undesirable water-interaction behaviour. PC/5LPs was chosen because low LPs loading improved film elasticity and maintained favourable barrier and surface properties, whereas higher LPs concentrations led to structural heterogeneities that negatively affected performance. These three formulations, therefore, represent the most balanced and functionally relevant candidates for further analysis and evaluation as packaging materials. The selected BSG-based film formulations and the proposed interactions between their components are shown in Fig. 3E.

3.4.6. Morphological, thermal, and structural properties of the selected BSG-based films

The surface and cross-section morphologies of the selected films (PC/0, PC/5AL, and PC/5LPs) were evaluated by SEM (Fig. 4A). PC/0 exhibited a smooth, homogeneous surface with a compact, continuous

Table 4
Water interaction and mechanical properties of the BSG-PC-based films.

Film	Water solubility (%)	WVP (10^{-8} × g/s m Pa)	WCA (°)	Tensile strength (MPa)	Elongation at break (%)	Young's modulus (MPa)
PC/0	88.2 ± 2.2^{b}	1.35 ± 0.24^{ab}	28.90 ± 1.93^{c}	2.3 ± 0.2^{d}	3.9 ± 0.5^{d}	173.9 ± 13.8^{b}
PC/5AL	87.6 ± 2.8^{b}	1.67 ± 0.19^{b}	26.66 ± 4.77^{bc}	1.6 ± 0.4^{b}	0.5 ± 0.1^{a}	412.5 ± 31.7^{d}
PC/10AL	90.3 ± 3.3^{b}	1.55 ± 0.19^{b}	38.46 ± 5.62^{d}	1.9 ± 0.5^{bc}	0.8 ± 0.3^{a}	319.1 ± 41.6^{c}
PC/15AL	91.8 ± 4.0^{b}	2.15 ± 0.46^{c}	39.00 ± 5.25^{d}	2.0 ± 0.3^{cd}	2.6 ± 0.5^{c}	161.0 ± 26.3^{b}
PC/5LPs	47.6 ± 3.1^{a}	1.14 ± 0.12^{a}	27.12 ± 3.81^{c}	1.7 ± 0.05^{bc}	4.8 ± 0.5^{e}	92.3 ± 7.2^{a}
PC/10LPs	48.0 ± 6.0^{a}	1.31 ± 0.23^{ab}	20.79 ± 2.43^{ab}	1.8 ± 0.05^{bc}	1.9 ± 0.2^{b}	171.6 ± 12.4^{b}
PC/15LPs	52.2 ± 8.0^{a}	1.53 ± 0.38^{b}	19.66 ± 2.81^{a}	1.1 ± 0.3^{a}	0.6 ± 0.1^{a}	188.0 ± 35.9^{b}

Statistically significant differences are illustrated by means followed by different letters in the same column (*p-value* < *0.05*).
BSG, brewers' spent grain; PC, protein concentrate; AL, alkaline lignin; LPs, lignin particles; WVP, water vapour permeability; WCA, water contact angle.

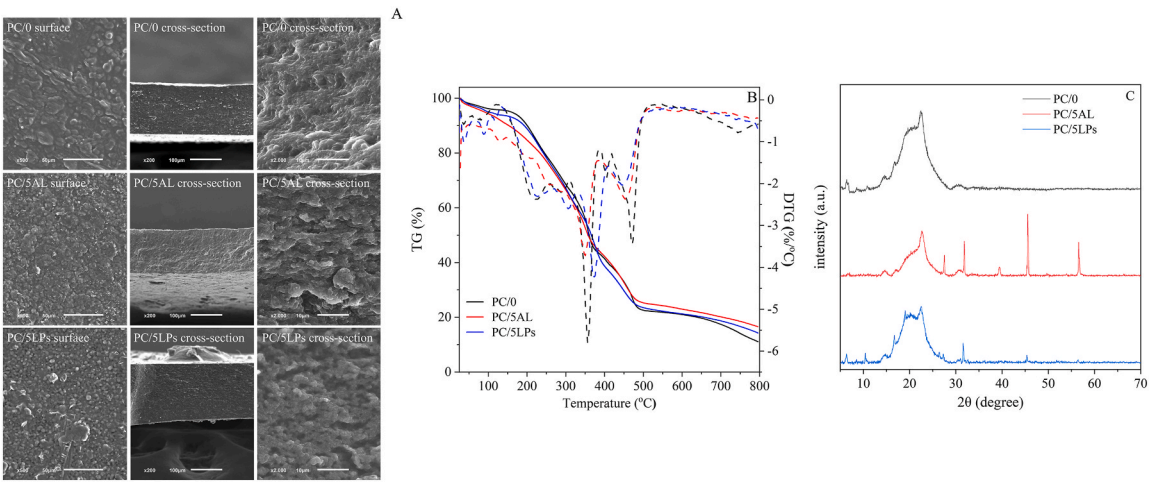

Fig. 4. A. Scanning electron microscopy, B. thermal decomposition (TG; solid lines) and derived thermogravimetry (DTG; dashed lines) curves, and C. X-ray diffraction pattern of the selected BSG-based films (PC/0, PC/5AL and PC/5LPs). PC; protein concentrate; AL, alkaline lignin; LPs, lignin particles.

cross-section, without noticeable cracks, confirming the good film-forming ability of the BSG-PC matrix (Qazanfarzadeh et al., 2024). In contrast, PC/5AL showed a slightly rougher surface and a more heterogeneous internal structure, with irregularities and micro-domains, indicating partial AL aggregation within the matrix. PC/5LPs displayed a rougher surface and a cross-section containing well-distributed particulate domains, suggesting better affinity of LPs, in line with the FTIR analysis. The presence of particle clusters (average size 3.0 ± 0.7 μm) within the continuous matrix indicates LP agglomerates formed during film casting and drying. Such aggregation is commonly observed in lignin-based systems and reflects the tendency of LPs to cluster within biopolymer matrices (Boarino & Klok, 2023). Globally, similar morphological features have been reported in other studies on BSG-based or lignin-reinforced protein films, where lignin aggregation leads to heterogeneous microstructures and altered surface topography (Rojas-Lema et al., 2023; Zadeh et al., 2018; W. Zhang et al., 2022). The EDS analysis confirmed sodium as the major inorganic element in all films, originating from the NaOH used to adjust the pH during BSG-PC solubilisation for film preparation (Fig. S1). Silicon was also detected, originating from the native BSG (Castro & Colpini, 2021). Sulfur signal was attributed to the S=O-containing groups naturally present in the BNC structure, whereas chloride signal was attributed to residual salts retained from the recovery process of BSG-PC. In the case of LPs-loaded films, phosphorus was also detected, consistent with the phosphate-citrate buffer used during LP formulation.

The TG and DTG curves of PC/0, PC/5AL and PC/5LPs films are presented in Fig. 4B. The first main degradation step of PC/0 at 221.7 °C corresponded to the degradation of BNC and glycerol (Rojas-Lema et al., 2023; Sarafidou, Vlysidis, et al., 2025), followed by peaks at 290.7 °C, 358.7 °C, and 471.5 °C, associated with the degradation of the protein, lignin and residues, respectively (Gbenebor et al., 2023; Jaguey-Hernández et al., 2023). The thermal behavior of the films significantly changed for PC/5AL and PC/5LPs. The incorporation of 5 % AL decreased the main decomposition temperatures to 197.3 °C, 279.2 °C, and 348.8 °C, indicating reduced thermal stability. These shifts reflect weaker cohesive interactions within the polymer network. Since BSG-derived lignin normally decomposes at higher temperatures (333-422 °C) (Gbenebor et al., 2023), the earlier degradation of PC/5AL indicates that AL disrupts the organisation of the BSG-PC matrix and weakens cohesive interactions, leading to reduced thermal stability. Although FTIR confirmed that AL forms hydrogen-bonding and intramolecular interactions with BSG-PC, its molecular dispersion and partial aggregation reorganize the matrix, disrupting chain packing. As a result, fewer stabilizing bonds must be broken during heating, lowering the energy required for thermal degradation. This interpretation is consistent with the higher WVP values, and the heterogeneous morphology observed for PC/5AL. In contrast, a significant increase of the decomposition temperatures occurred by the 5 % LPs addition up to 228.7 °C, 306.7 °C, and 372.4 °C, demonstrating enhanced thermal stability. This improvement aligns with the structural reorientation occurring during LP formation, which exposes polar acetyl groups capable of forming hydrogen bonds with protein functional groups and promoting local organisation. As a result, LPs act as well-distributed particulate micro-domains that restrict chain mobility and increase the energy required for thermal degradation. Enhanced degradation temperature upon LPs addition have been reported in the literature, attributed to their good dispersion within the matrix, highlighting the importance of lignin morphology and hydrogen-bond formation in the thermal performance of biopolymer films (Rojas-Lema et al., 2023).

XRD analysis was performed to evaluate whether lignin incorporation altered the structural organization of the bio-based films. All diffractograms exhibited broad, low-intensity diffraction peaks typical of amorphous biopolymer matrices, confirming the absence of long-range crystalline order (Fig. 4C). A broad peak centered at 2θ = 22.5° was observed in all samples and is attributed to the contribution of *Iα* crystalline domains associated with BNC (Sarafidou, Vlysidis, et al., 2025), together with the amorphous background originating from the BSG-PC matrix (Gbenebor et al., 2023). Quantitative analysis showed that PC/0 exhibited a crystallinity of 49.6 %, consistent with the amorphous nature of BSG-PC (Ribeiro-Sanches et al., 2026). The addition of AL reduced crystallinity to 42.3 %, suggesting that AL interferes with the local ordering of BSG-PC chains, likely due to its molecular dispersion and disruption of intermolecular packing. These morphological features are consistent with the SEM microstructure and the weaker cohesive bonding inferred from TG. In contrast, films containing LPs showed a slightly higher crystallinity (53.0 %), which may be attributed to the particulate nature of LPs. This interpretation aligns with the enhanced elongation at break observed for PC/5LPs and with previous studies reporting morphology-dependent effects of lignin on protein-based films (Zadeh et al., 2018).

Overall, AL and LPs interact with the BSG-PC matrix through distinct structural mechanisms. AL forms hydrogen-bonding and other intramolecular interactions with BSG-PC, which reorganize the network, and disrupt the intermolecular packing of the matrix, reducing the main degradation temperatures and elasticity. In contrast, LPs create well-distributed particulate micro-domains within the protein network, enhancing thermal stability, promoting local structural organisation, and improving matrix compactness.

3.4.7. Application of bio-based packaging materials on salmon fillets

3.4.7.1. Microbiological analysis. Salmon was selected as a case study for the application of BSG-based films because of its high nutritional value, appealing colour, and flavour, and short shelf-life, which is attributed to microbial spoilage and the oxidation of polyunsaturated fatty acids (Romero et al., 2022; Yan et al., 2022). In the present study, salmon fillets were placed into plastic cups sealed with PVC, PC/0, PC/5AL, and PC/5LPs films to evaluate their packaging performance (Fig. S2). Fig. 5 represents the microbial growth of TMC, *Pseudomonas* spp. and Enterobacteriaceae fitted to the Baranyi Growth Model for the applied packaging systems. Initial TMC was 5.1 log (CFU/g), indicating a relatively high microbial load, and the samples entered the exponential growth phase immediately. The highest microbial growth rate for TMC was observed in fillets packed with PVC (0.94 $days^{-1}$), followed by PC/5AL and PC/0 (0.82 and 0.79 $days^{-1}$, respectively; *p-value* > *0.05*) (Table 5). After 9 days of storage at 4 °C, the highest final microbial load was observed in salmon fillets packed with PVC (9.59 log (CFU/g)), followed by PC/0 and PC/5AL (8.60 log (CFU/g); *p-value* > *0.05*).

The microbial growth rate and the maximum specific growth rate (N_{max}) of Pr/5LPs were significantly lower (0.50 $days^{-1}$ and 7.72 log (CFU/g), respectively), indicating microbial growth inhibition. A similar trend was observed for *Pseudomonas* spp., where the lowest microbial growth rate was reported in the PC/5LPs-packed fillets (0.35 $days^{-1}$ and 7.32 log (CFU/g)), followed by PC/5AL (0.47 $days^{-1}$ and 7.19 log (CFU/g)), with no significant differences (*p-value* > *0.05*). While lignin has been reported to possess antimicrobial properties and especially LPs (Luzi et al., 2021), the structural differences between the bio-based films and the packaging configuration used in this study suggest that the reduced microbial growth observed here is primarily associated with headspace-mediated effects rather than direct antimicrobial action. In the applied salmon storage setup, the films were positioned on the inner

Table 5
Kinetic parameters of microbial growth for total aerobic mesophilic counts, *Pseudomonas* spp. and Enterobacteriaceae in salmon fillets packed with PVC and BSG-based films.

	k ($days^{-1}$)	N_{max} (log (CFU/g))	R^2
Total aerobic mesophilic counts			
PVC	0.94 ± 0.06^{b}	9.59 ± 0.12^{c}	0.99
PC/0	0.79 ± 0.03^{b}	8.60 ± 0.06^{b}	1.00
PC/5AL	0.82 ± 0.13^{b}	8.60 ± 0.21^{b}	0.94
PC/5LPs	0.50 ± 0.06^{a}	7.72 ± 0.21^{a}	0.97
Pseudomonas spp.			
PVC	0.77 ± 0.04^{b}	8.12 ± 0.20^{b}	0.91
PC/0	0.74 ± 0.11^{b}	8.22 ± 0.14^{b}	0.97
PC/5AL	0.47 ± 0.07^{ab}	7.19 ± 0.19^{a}	0.91
PC/5LPs	0.35 ± 0.08^{a}	7.32 ± 0.27^{a}	0.93
Enterobacteriaceae			
PVC	0.77 ± 0.11^{a}	5.62 ± 0.24^{a}	0.96
PC/0	0.70 ± 0.04^{a}	5.62 ± 0.11^{a}	0.99
PC/5AL	0.65 ± 0.06^{a}	5.36 ± 0.14^{a}	0.98
PC/5LPs	0.61 ± 0.12^{a}	5.16 ± 0.31^{a}	0.91

Different subscript letters between the same parameter (column) indicate statistically significant differences (*p-value* < *0.05*). PVC, Polyvinyl chloride (PVC); BSG, brewers' spent grain; PC, protein concentrate; AL, alkaline lignin; LPs, lignin particles, microbial growth rate (k), and maximum specific growth rate (N_{max}).

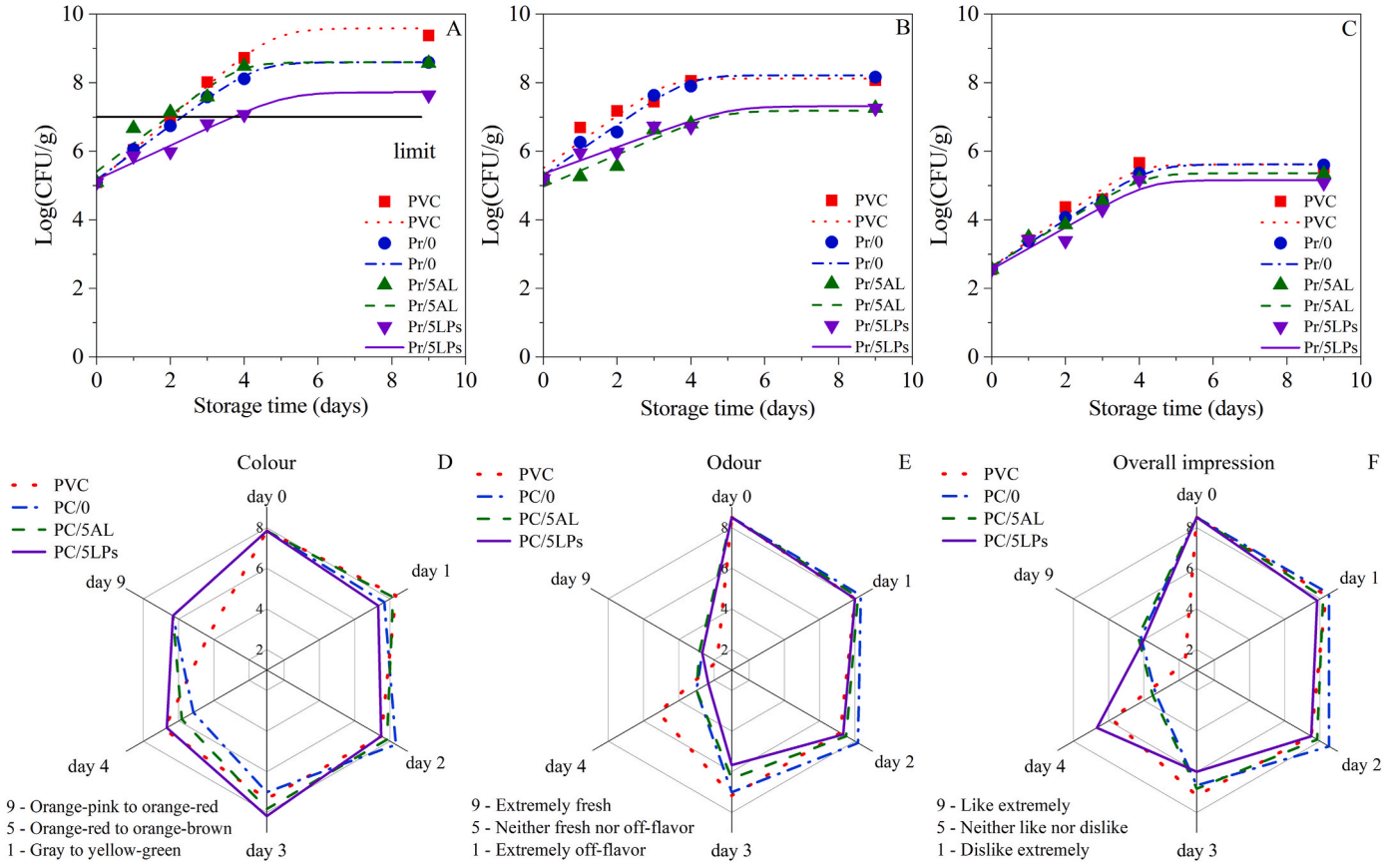

Fig. 5. Shelf-life (A. Total Aerobic Mesophilic Count, B. *Pseudomonas* spp. and C. Enterobacteriaceae) and sensory analysis (D. colour, E. odour, and F. overall impression) of the packed salmon fillets during the 9-days cold storage period (5 °C). PVC (red-dotted line/square), PC/0 (blue-dashed line/circle), PC/5AL (green-dashed-dotted line/triangle) and P5CLP (purple-solid line/inverted triangle). PC; protein concentrate; AL, alkaline lignin; LPs, lignin particles. (For interpretation of the references to colour in this figure legend, the reader is referred to the Web version of this article.)

side of the package lid and did not contact the fish surface; therefore, any influence on microbial growth likely arises from modifications of the headspace microenvironment rather than diffusion of active compounds (Azevedo et al., 2022). In case of Enterobacteriaceae, no significant differences were observed on either microbial growth rates or maximum microbial load between Enterobacteriaceae count. The shelf-life of salmon fillets at 4 °C packed with PVC, PC/0 and PC/5AL was 2 days, whereas PC/5LPs extended the shelf-life up to 4 days, based on the acceptability limit of 10^7 CFU/g (ICMSF, 1986).

The antimicrobial activity of lignin has been previously reported in the literature (Alzagameem et al., 2019; K. Li et al., 2023), attributed to phenolic structures capable of inducing oxidative stress, membrane perturbation, or metabolic interference (Ndaba et al., 2020). In addition to these intrinsic properties, lignin-containing films have also been shown to influence the headspace microenvironment during storage (Mohammad Zadeh et al., 2019). In the present study, the reduced bacterial growth observed during storage therefore reflects the overall packaging configuration.

3.4.7.2. Sensory analysis. Fig. 5D–F indicate means of sensory scores for colour, odour, overall impression of all packed salmon fillets over a 9-day period of storage at 4 °C. Colour scores ranged between 7.0 and 8.3 during the first 3 days of storage. In contrast, by increasing the storage time up to 4 days, the colour score decreased up to 5.5-6.8. The initial odour scores were high (8.0-8.5 on days 0 and 1). After 2 days of storage, however, the sensory panel detected a transferable lignin-like odour in samples packed with PC/5L and PC/5LPs, resulting in an odour score reduction of up to 5.7. Overall, all samples remained within acceptable sensory limits up to day 4. Nevertheless, the shelf-life as determined by microbial growth was limited to 2 days for fillets packaged with PVC, PC/0, PC/5L and extended to 4 days for PC/5LPs. These results indicate that bio-based films can be applied as alternative packaging materials without compromising product quality, while the use of PC/5LPs may further extend the shelf-life by an additional 2 days.

4. Conclusions

The effective valorisation of brewing industry side-streams was demonstrated for the development of bio-based food packaging by using the major fractions derived from the process. BSG was successfully converted into a carbon-rich hydrolysate for BC production. At the same time, the BSG-RS were valorised to recover protein- and lignin-rich fractions, identified as the optimal route for film formulation. The recovered BSG-PC served as the matrix for BSG-based films, and the isolated lignin was incorporated as a functional agent in two forms (AL and LPs) at 5 %, 10 %, and 15 % (w/w). The produced films exhibited excellent light-barrier properties ($T_{600} < 2.3$ %) and antioxidant activity (up to 40 % DPPH inhibition). Structural analyses further revealed that AL and LPs interact with the protein matrix through distinct morphology-dependent mechanisms that lead to opposite effects on structural organisation and thermal stability. A shelf-life case study with salmon fillets confirmed the films' potential for use in food packaging. Samples packed with PC/5LPs extended shelf life by two additional days compared to PVC, PC/0, and PC/5AL (4 days vs 2 days at 4 °C). Overall, the BSG-derived films demonstrate promising functional and active properties, supporting their potential use as sustainable alternatives to conventional plastic packaging. However, films were evaluated under specific storage and environmental conditions, and broader testing across different humidity levels, temperatures, and food types would be needed to confirm their wider applicability. In addition, higher lignin loadings showed limited compatibility with the protein matrix and did not enhance mechanical performance, indicating that further optimisation of lignin incorporation strategies is necessary. Future studies using complementary structural analyses could help elucidate the microstructural factors underlying this behavior.

CRediT authorship contribution statement

Christos Margioulas: Writing – original draft, Methodology, Investigation, Formal analysis, Data curation. **Mirva Sarafidou:** Writing – review & editing, Writing – original draft, Validation, Methodology, Investigation, Formal analysis, Data curation. **Giovana Colucci:** Writing – review & editing, Validation, Investigation. **Arantzazu Santamaria-Echart:** Writing – review & editing, Validation, Conceptualization. **Chrysanthi Argeiti:** Validation, Formal analysis. **Spiros Paramithiotis:** Writing – review & editing, Data curation, Conceptualization. **Theofania Tsironi:** Writing – review & editing, Resources, Data curation, Conceptualization. **Apostolis Koutinas:** Writing – review & editing, Resources, Project administration, Funding acquisition, Conceptualization. **Maria-Filomena Barreiro:** Writing – review & editing, Supervision, Resources, Project administration, Funding acquisition, Conceptualization. **Katiana Filippi:** Writing – review & editing, Supervision, Data curation, Conceptualization.

Declaration of competing interest

The authors declare that they have no known competing financial interests or personal relationships that could have appeared to influence the work reported in this paper.

Acknowledgments

The authors would like to acknowledge COST Action CA17128 "Establishment of a Pan-European Network on the Sustainable Valorisation of Lignin (LignoCOST)". LignoCOST was supported by COST (European Cooperation in Science and Technology), in promoting interaction, exchange of knowledge and collaborations in the field of lignin valorisation. More information can be found at www.lignocost.eu. The authors would also like to acknowledge financial support from the BioSupPack Project under the European Union's Horizon 2020 Framework Programme under Grant agreement no. 101023685 entitled "Demonstrative process for the production and enzymatic recycling of environmentally safe, superior and versatile PHA-based rigid packaging solutions by plasma integration in the value chain (Acronym: BioSupPack Project). Additional funding for this project has been received from the Foundation for Science and Technology (FCT, Portugal) through national funds FCT/MCTES (PIDDAC) to CIMO UID/00690/2025 (10.54499/UID/00690/2025) and UID/PRR/00690/2025 (10.54499/UID/PRR/00690/2025); and SusTEC, LA/P/0007/2020 (DOI: 10.54499/LA/P/0007/2020). FCT for the Ph.D. research grant of G. Colucci (2021.05215.BD, DOI: 10.54499/2021.05215.BD) and the institutional scientific employment program contract of A. Santamaria-Echart.

Appendix A. Supplementary data

Supplementary data to this article can be found online at https://doi.org/10.1016/j.foodhyd.2026.112854.

Data availability

Data will be made available on request.

References

Alzagameem, A., Klein, S. E., Bergs, M., Do, X. T., Korte, I., Dohlen, S., Hüwe, C., Kreyenschmidt, J., Kamm, B., Larkins, M., & Schulze, M. (2019). Antimicrobial activity of lignin and lignin-derived cellulose and chitosan composites against selected pathogenic and spoilage microorganisms. *Polymers, 11*(4), 670. https://doi.org/10.3390/polym11040670

Argeiti, C., Psaki, O., Filippi, K., Ladakis, D., Scally, L., Cullen, P. J., Koutinas, A., & Stylianou, E. (2024). Biorefinery electrification of brewers' spent grains using plasma bubbles for sustainable production of poly(3-hydroxybutyrate). *Chemical Engineering Journal, 496*, Article 153548. https://doi.org/10.1016/j.cej.2024.153548

ASTM D5946. (2017). *Standard Test method for corona-treated polymer films using water contact angle measurements*. West Conshohocken, PA, USA: ASTM International, 2017 https://www.astm.org/d5946-17.html.

Athanasopoulou, E., Katsiroumpa, A., Gardeli, C., & Tsironi, T. (2025). Comparative study of packaging materials developed from fish and legume protein concentrates. *Future Foods, 11*, Article 100563. https://doi.org/10.1016/j.fufo.2025.100563

Azevedo, A. G., Barros, C., Miranda, S., Machado, A. V., Castro, O., Silva, B., Saraiva, M., Silva, A. S., Pastrana, L., Carneiro, O. S., & Cerqueira, M. A. (2022). Active flexible films for food packaging: A review. *Polymers, 14*(12), 2442. https://doi.org/10.3390/polym14122442

Baranyi, J., & Roberts, T. A. (1995). Mathematics of predictive food microbiology. *International Journal of Food Microbiology, 26*(2), 199–218. https://doi.org/10.1016/0168-1605(94)00121-L

Basbasan, A. J., Hararak, B., Winotapun, C., Wanmolee, W., Leelaphiwat, P., Boonruang, K., Chinsirikul, W., & Chonhenchob, V. (2022). Emerging challenges on viability and commercialization of lignin in biobased polymers for food packaging: A review. *Food Packaging and Shelf Life, 34*, Article 100969. https://doi.org/10.1016/j.fpsl.2022.100969

Boarino, A., & Klok, H.-A. (2023). Opportunities and challenges for lignin valorization in food packaging, antimicrobial, and agricultural applications. *Biomacromolecules, 24*(3), 1065–1077. https://doi.org/10.1021/acs.biomac.2c01385

Bonifácio-Lopes, T., Vilas Boas, A. A., Coscueta, E. R., Costa, E. M., Silva, S., Campos, D., Teixeira, J. A., & Pintado, M. (2020). Bioactive extracts from brewer's spent grain. *Food & Function, 11*(10), 8963–8977. https://doi.org/10.1039/D0FO01426E

Botta, J. R. (1996). *Evaluation of seafood freshness quality*. John Wiley & Sons.

Calva-Estrada, S. J., Jiménez-Fernández, M., & Lugo-Cervantes, E. (2019). Protein-Based films: Advances in the development of biomaterials applicable to food packaging. *Food Engineering Reviews, 11*(2), 78–92. https://doi.org/10.1007/s12393-019-09189-w

Carvalheiro, F. (2004). Production of oligosaccharides by autohydrolysis of brewery's spent grain. *Bioresource Technology, 91*(1), 93–100. https://doi.org/10.1016/S0960-8524(03)00148-2

Castro, L. E. N., & Colpini, L. M. S. (2021). All-around characterization of brewers' spent grain. *European Food Research and Technology, 247*(12), 3013–3021. https://doi.org/10.1007/s00217-021-03860-5

Celus, I., Brijs, K., & Delcour, J. A. (2007). Enzymatic hydrolysis of brewers' spent grain proteins and technofunctional properties of the resulting hydrolysates. *Journal of Agricultural and Food Chemistry, 55*(21), 8703–8710. https://doi.org/10.1021/jf071793c

Colucci, G., Santamaria-Echart, A., Silva, S. C., Teixeira, L. G., Ribeiro, A., Rodrigues, A. E., & Barreiro, M. F. (2023). Development of colloidal lignin particles through particle design strategies and screening of their Pickering stabilizing potential. *Colloids and Surfaces A: Physicochemical and Engineering Aspects, 666*, Article 131287. https://doi.org/10.1016/j.colsurfa.2023.131287

De Sousa Nascimento, L., Da Mata Vieira, F. I. D., Horácio, V., Marques, F. P., Rosa, M. F., Souza, S. A., De Freitas, R. M., Uchoa, D. E. A., Mazzeto, S. E., Lomonaco, D., & Avelino, F. (2021). Tailored organosolv banana peels lignins: Improved thermal, antioxidant and antimicrobial performances by controlling process parameters. *International Journal of Biological Macromolecules, 181*, 241–252. https://doi.org/10.1016/j.ijbiomac.2021.03.156

Devnani, B., Moran, G. C., & Grossmann, L. (2023). Extraction, composition, functionality, and utilization of brewer's spent grain protein in food formulations. *Foods, 12*(7), 1543. https://doi.org/10.3390/foods12071543

Efthymiou, M.-N., Tsouko, E., Papagiannopoulos, A., Athanasoulia, I.-G., Georgiadou, M., Pispas, S., Briassoulis, D., Tsironi, T., & Koutinas, A. (2022a). Development of biodegradable films using sunflower protein isolates and bacterial nanocellulose as innovative food packaging materials for fresh fruit preservation. *Scientific Reports, 12*(1), 6935. https://doi.org/10.1038/s41598-022-10913-6

Efthymiou, M.-N., Tsouko, E., Pateraki, C., Papagiannopoulos, A., Tzamalis, P., Pispas, S., Bethanis, K., Mantala, I., & Koutinas, A. (2022b). Property evaluation of bacterial cellulose nanostructures produced from confectionery wastes. Biochemical Engineering Journal, 186, Article 108575. 10.1016/j.bej.2022.108575.

Ferreira, A. M., Martins, J., Carvalho, L. H., & Magalhães, F. D. (2019). Biosourced disposable trays made of brewer's spent grain and potato starch. *Polymers, 11*(5), 923. https://doi.org/10.3390/polym11050923

Filippi, K., Georgaka, N., Alexandri, M., Papapostolou, H., & Koutinas, A. (2021). Valorisation of grape stalks and pomace for the production of bio-based succinic acid by Actinobacillus succinogenes. *Industrial Crops and Products, 168*, Article 113578. https://doi.org/10.1016/j.indcrop.2021.113578

Filippi, K., Ladakis, D., Ioannidou, S. M., Stylianou, E., Baltatzis, G. E., Trougakos, I. P., Cullen, P. J., & Koutinas, A. (2025). Bioprocess development and life cycle assessment of succinic acid production from grape stalks incorporating electricity-driven technologies. *Journal of Environmental Chemical Engineering, 13*(5), Article 117803. https://doi.org/10.1016/j.jece.2025.117803

Filippi, K., Papapostolou, H., Alexandri, M., Vlysidis, A., Myrtsi, E. D., Ladakis, D., Pateraki, C., Haroutounian, S. A., & Koutinas, A. (2022). Integrated biorefinery development using winery waste streams for the production of bacterial cellulose, succinic acid and value-added fractions. *Bioresource Technology, 343*, Article 125989. https://doi.org/10.1016/j.biortech.2021.125989

Gbenebor, O. P., Olanrewaju, O. A., Usman, M. A., & Adeosun, S. O. (2023). Lignin from brewers' spent grain: Structural and thermal evaluations. *Polymers, 15*(10), 2346. https://doi.org/10.3390/polym15102346

Gregory, D. A., Tripathi, L., Fricker, A. T. R., Asare, E., Orlando, I., Raghavendran, V., & Roy, I. (2021). Bacterial cellulose: A smart biomaterial with diverse applications. *Materials Science and Engineering: R: Reports, 145*, Article 100623. https://doi.org/10.1016/j.mser.2021.100623

Gupta, R. K., Guha, P., & Srivastav, P. P. (2022). Natural polymers in bio-degradable/edible film: A review on environmental concerns, cold plasma technology and nanotechnology application on food packaging- A recent trends. *Food Chemistry Advances, 1*, Article 100135. https://doi.org/10.1016/j.focha.2022.100135

He, X., Luzi, F., Hao, X., Yang, W., Torre, L., Xiao, Z., Xie, Y., & Puglia, D. (2019). Thermal, antioxidant and swelling behaviour of transparent polyvinyl (alcohol) films in presence of hydrophobic citric acid-modified lignin nanoparticles. *International Journal of Biological Macromolecules, 127*, 665–676. https://doi.org/10.1016/j.ijbiomac.2019.01.202

He, Y., Ye, H.-C., You, T.-T., & Xu, F. (2023). Sustainable and multifunctional cellulose-lignin films with excellent antibacterial and UV-shielding for active food packaging. *Food Hydrocolloids, 137*, Article 108355. https://doi.org/10.1016/j.foodhyd.2022.108355

ICMSF. (1986). International commission on microbiological specifications for foods, sampling plans for fish and shellfish. In *ICMSF, microorganisms in foods, sampling for microbiological analysis: Principles and scientific applications* (2nd ed.). Toronto, ON, Canada: University of Toronto Press.

Ikram, S., Huang, L., Zhang, H., Wang, J., & Yin, M. (2017). Composition and nutrient value proposition of brewers spent grain. *Journal of Food Science, 82*(10), 2232–2242. https://doi.org/10.1111/1750-3841.13794

Ioannidou, S. M., Pateraki, C., Ladakis, D., Papapostolou, H., Tsakona, M., Vlysidis, A., Kookos, I. K., & Koutinas, A. (2020). Sustainable production of bio-based chemicals and polymers via integrated biomass refining and bioprocessing in a circular bioeconomy context. *Bioresource Technology, 307*, Article 123093. https://doi.org/10.1016/j.biortech.2020.123093

Jaguey-Hernández, Y., Tapia-Ignacio, C., Aguilar-Arteaga, K., González-Olivares, L. G., Castañeda-Ovando, E. P., Cruz-Cansino, N., Ojeda-Ramirez, D., & Castañeda-Ovando, A. (2023). Thermoplastic biofilms obtained from an arabinoxylan-rich fraction from brewers' spent grain: Physicochemical characterization and thermal analysis. *Biomass Conversion and Biorefinery, 13*(15), 14035–14047. https://doi.org/10.1007/s13399-021-02288-x

Junttila, M. H. (2022). Extraction of brewers' spent grain in near subcritical conditions: A method to obtain high protein contents extracts. *Journal of Agriculture and Food Research, 10*, Article 100378. https://doi.org/10.1016/j.jafr.2022.100378

Li, X., Yang, J., Khan, M. R., Ahmad, N., & Zhang, W. (2025). Dopamine-polyphenol self-assembled nanoparticle functionalized soy protein isolate films. *Chemical Engineering Journal, 524*, Article 169424. https://doi.org/10.1016/j.cej.2025.169424

Li, K., Zhong, W., Li, P., Ren, J., Jiang, K., & Wu, W. (2023). Antibacterial mechanism of lignin and lignin-based antimicrobial materials in different fields. *International Journal of Biological Macromolecules, 252*, Article 126281. https://doi.org/10.1016/j.ijbiomac.2023.126281

Llana-Ruiz-Cabello, M., Gutiérrez-Praena, D., Puerto, M., Pichardo, S., Jos, Á., & Cameán, A. M. (2015). In vitro pro-oxidant/antioxidant role of carvacrol, thymol and their mixture in the intestinal Caco-2 cell line. *Toxicology in Vitro, 29*(4), 647–656. https://doi.org/10.1016/j.tiv.2015.02.006

López-Linares, J. C., Lucas, S., García-Cubero, M. T., Jiménez, J. J., & Coca, M. (2020). A biorefinery based on brewer's spent grains: Arabinoxylans recovery by microwave assisted pretreatment integrated with butanol production. *Industrial Crops and Products, 158*, Article 113044. https://doi.org/10.1016/j.indcrop.2020.113044

Lu, X., Gu, X., & Shi, Y. (2022). A review on lignin antioxidants: Their sources, isolations, antioxidant activities and various applications. *International Journal of Biological Macromolecules, 210*, 716–741. https://doi.org/10.1016/j.ijbiomac.2022.04.228

Luzi, F., Yang, W., Ma, P., Torre, L., & Puglia, D. (2021). Lignin-based materials with antioxidant and antimicrobial properties. In *Lignin-Based materials for biomedical applications* (pp. 291–326). Elsevier. https://doi.org/10.1016/B978-0-12-820303-3.00003-5.

Lynch, K. M., Steffen, E. J., & Arendt, E. K. (2016). Brewers' spent grain: A review with an emphasis on food and health. *Journal of the Institute of Brewing, 122*(4), 553–568. https://doi.org/10.1002/jib.363

Meneses, N. G. T., Martins, S., Teixeira, J. A., & Mussatto, S. I. (2013). Influence of extraction solvents on the recovery of antioxidant phenolic compounds from brewer's spent grains. *Separation and Purification Technology, 108*, 152–158. https://doi.org/10.1016/j.seppur.2013.02.015

Merino, D., Bertolacci, L., Paul, U. C., Simonutti, R., & Athanassiou, A. (2021). Avocado peels and seeds: Processing strategies for the development of highly antioxidant bioplastic films. *ACS Applied Materials & Interfaces, 13*(32), 38688–38699. https://doi.org/10.1021/acsami.1c09433

Mohammad Zadeh, E., O'Keefe, S. F., & Kim, Y. (2019). Lignin-Based biopolymeric active packaging System for oil products. *Journal of Food Science, 84*(6), 1420–1426. https://doi.org/10.1111/1750-3841.14632

Moreirinha, C., Vilela, C., Silva, N. H. C. S., Pinto, R. J. B., Almeida, A., Rocha, M. A. M., Coelho, E., Coimbra, M. A., Silvestre, A. J. D., & Freire, C. S. R. (2020). Antioxidant and antimicrobial films based on brewers spent grain arabinoxylans, nanocellulose and feruloylated compounds for active packaging. *Food Hydrocolloids, 108*, Article 105836. https://doi.org/10.1016/j.foodhyd.2020.105836

Mussatto, S. I., & Roberto, I. C. (2006). Chemical characterization and liberation of pentose sugars from brewer's spent grain. *Journal of Chemical Technology & Biotechnology, 81*(3), 268–274. https://doi.org/10.1002/jctb.1374

Ndaba, B., Roopnarain, A., Daramola, M. O., & Adeleke, R. (2020). Influence of extraction methods on antimicrobial activities of lignin-based materials: A review. *Sustainable Chemistry and Pharmacy, 18*, Article 100342. https://doi.org/10.1016/j.scp.2020.100342

Österberg, M., Sipponen, M. H., Mattos, B. D., & Rojas, O. J. (2020). Spherical lignin particles: A review on their sustainability and applications. *Green Chemistry, 22*(9), 2712–2733. https://doi.org/10.1039/D0GC00096E

Oztuna Taner, O., Ekici, L., & Akyuz, L. (2023). CMC-based edible coating composite films from Brewer's spent grain waste: A novel approach for the fresh strawberry package. *Polymer Bulletin, 80*(8), 9033–9058. https://doi.org/10.1007/s00289-022-04490-x

Pedro Silva, J., Sousa, S., Rodrigues, J., Antunes, H., Porter, J. J., Gonçalves, I., & Ferreira-Dias, S. (2004). Adsorption of acid orange 7 dye in aqueous solutions by spent brewery grains. *Separation and Purification Technology, 40*(3), 309–315. https://doi.org/10.1016/j.seppur.2004.03.010

Perrocheau, L., Rogniaux, H., Boivin, P., & Marion, D. (2005). Probing heat-stable water-soluble proteins from barley to malt and beer. *Proteomics, 5*(11), 2849–2858. https://doi.org/10.1002/pmic.200401153

Pinheiro, T., Coelho, E., Romaní, A., & Domingues, L. (2019). Intensifying ethanol production from brewer's spent grain waste: Use of whole slurry at high solid loadings. *New Biotechnology, 53*, 1–8. https://doi.org/10.1016/j.nbt.2019.06.005

Priyadarshi, R., Kim, S.-M., & Rhim, J.-W. (2021). Pectin/pullulan blend films for food packaging: Effect of blending ratio. *Food Chemistry, 347*, Article 129022. https://doi.org/10.1016/j.foodchem.2021.129022

Proaño, J. L., Salgado, P. R., Cian, R. E., Mauri, A. N., & Drago, S. R. (2020). Physical, structural and antioxidant properties of brewer's spent grain protein films. *Journal of the Science of Food and Agriculture, 100*(15), 5458–5465. https://doi.org/10.1002/jsfa.10597

Puligundla, P., & Mok, C. (2021). Recent advances in biotechnological valorization of brewers' spent grain. *Food Science and Biotechnology, 30*(3), 341–353. https://doi.org/10.1007/s10068-021-00900-4

Qazanfarzadeh, Z., Masek, A., Chakraborty, S., & Kumaravel, V. (2024). Development of brewer's spent grain-derived bio nanocomposites through a multiproduct biorefinery approach for food packaging. *Industrial Crops and Products, 220*, Article 119226. https://doi.org/10.1016/j.indcrop.2024.119226

Qin, F., Johansen, A. Z., & Mussatto, S. I. (2018). Evaluation of different pretreatment strategies for protein extraction from brewer's spent grains. *Industrial Crops and Products, 125*, 443–453. https://doi.org/10.1016/j.indcrop.2018.09.017

Ribeiro-Sanches, M. A., Júnior, S. L. F., Santezi, C., Caruso, Í. P., Augusto, P. E. D., Telis-Romero, J., & Polachini, T. C. (2026). Extraction of proteins from brewer's spent grain using ultrasound and alkaline hydrogen peroxide: Impact on extraction yield, structural and techno-functional properties. *Food Hydrocolloids, 172*, Article 112012. https://doi.org/10.1016/j.foodhyd.2025.112012

Rojas-Chamorro, J. A., Romero, I., López-Linares, J. C., & Castro, E. (2020). Brewer's spent grain as a source of renewable fuel through optimized dilute acid pretreatment. *Renewable Energy, 148*, 81–90. https://doi.org/10.1016/j.renene.2019.12.030

Rojas-Lema, S., Nilsson, K., Langton, M., Trifol, J., Gomez-Caturla, J., Balart, R., Garcia-Garcia, D., & Moriana, R. (2023). The effect of pine cone lignin on mechanical, thermal and barrier properties of faba bean protein films for packaging applications. *Journal of Food Engineering, 339*, Article 111282. https://doi.org/10.1016/j.jfoodeng.2022.111282

Romero, J., Cruz, R. M. S., Díez-Méndez, A., & Albertos, I. (2022). Valorization of berries' agro-industrial waste in the development of biodegradable Pectin-based films for fresh salmon (Salmo salar) shelf-life monitoring. *International Journal of Molecular Sciences, 23*(16), 8970. https://doi.org/10.3390/ijms23168970

Santos, M. V., Ranalli, N., Orjuela-Palacio, J., & Zaritzky, N. (2024). Brewers spent grain drying: Drying kinetics, moisture sorption isotherms, bioactive compounds stability and Bacillus cereus lethality during thermal treatment. *Journal of Food Engineering, 364*, Article 111796. https://doi.org/10.1016/j.jfoodeng.2023.111796

Sarafidou, M., Forys, A., Godzierz, M., Kobyliukh, A., Trzebicka, B., Pispas, S., Koutinas, A., & Tsouko, E. (2025). Modification of bacterial nanocellulose using nonthermal plasma-assisted enzymatic hydrolysis. *Biomacromolecules, 26*(9), 5657–5669. https://doi.org/10.1021/acs.biomac.5c00397

Sarafidou, M., Tsouko, E., Giannoulis, A., Briassoulis, D., Baltatzis, G. E., Trougakos, I. P., Tsironi, T., & Koutinas, A. (2025). Engineering pectin biobased films with bacterial cellulose nanostructures for enhanced food packaging performance. *ACS Food Science & Technology, 5*(9), 3374–3386. https://doi.org/10.1021/acsfoodscitech.5c00405

Sarafidou, M., Vlysidis, A., Papapetros, K., Filippi, K., Voyiatzis, G., Andrikopoulos, K. S., Koutinas, A., & Stylianou, E. (2025). Development and characterization of bacterial cellulose nanocomposites from de-pectinated sugar beet pulp hydrolysates within a biorefinery. *Bioresource Technology, 427*, Article 132351. https://doi.org/10.1016/j.biortech.2025.132351

Sganzerla, W. G., Ampese, L. C., Mussatto, S. I., & Forster-Carneiro, T. (2021). A bibliometric analysis on potential uses of brewer's spent grains in a biorefinery for the circular economy transition of the beer industry. *Biofuels, Bioproducts and Biorefining, 15*(6), 1965–1988. https://doi.org/10.1002/bbb.2290

Shroti, G. K., & Saini, C. S. (2022). Development of edible films from protein of brewer's spent grain: Effect of pH and protein concentration on physical, mechanical and barrier properties of films. *Applied Food Research, 2*(1), Article 100043. https://doi.org/10.1016/j.afres.2022.100043

Silva, L., Colussi, F., Martins, J. T., Vieira, J. M., Pastrana, L. M., Teixeira, J. A., Cerqueira, M. A., & Michelin, M. (2024). Strategies for the incorporation of organosolv lignin in hydroxypropyl methylcellulose-based films: A comparative study. *International Journal of Biological Macromolecules, 280*, Article 135498. https://doi.org/10.1016/j.ijbiomac.2024.135498

Silva, K. F., Marques, C. S., De Freitas Junior, A., Dias, M. V., & Mori, F. A. (2023). Whey protein isolate and kraft lignin multifunctional films for potential food packaging application: UV block and antioxidant potential. *Food Bioscience, 53*, Article 102581. https://doi.org/10.1016/j.fbio.2023.102581

Sluiter, A., Hames, B., Ruiz, R., Scarlata, C., Sluiter, J., & Templeton, D. (2008a). *Determination of ash in biomass: Laboratory analytical procedure (LAP)*. https://www.nrel.gov/docs/gen/fy08/42622.pdf.

Sluiter, A., Hames, B., Ruiz, R., Scarlata, C., Sluiter, J., Templeton, D., & Crocker, D. (2008b). *Determination of structural carbohydrates and lignin in biomass: Laboratory analytical procedure (LAP) (Revised July 2011)*. http://www.nrel.gov/biomass/analytical_procedures.html.

Sluiter, A., Ruiz, R., Scarlata, C., Sluiter, J., & Templeton, D. (2008c). *Determination of extractives in biomass: Laboratory analytical procedure (LAP); Issue Date 7/17/2005*. http://www.nrel.gov/biomass/analytical_procedures.html.

Socaci, S. A., Fărcaș, A. C., Diaconeasa, Z. M., Vodnar, D. C., Rusu, B., & Tofană, M. (2018). Influence of the extraction solvent on phenolic content, antioxidant, antimicrobial and antimutagenic activities of brewers' spent grain. *Journal of Cereal Science, 80*, 180–187. https://doi.org/10.1016/j.jcs.2018.03.006

Statista. (2025). Annual production of plastics worldwide from 1950 to 2023. https://www.statista.com/statistics/282732/global-production-of-plastics-since-1950/#statisticContainer.

Tsironi, T. N., & Taoukis, P. S. (2017). Effect of storage temperature and osmotic pre-treatment with alternative solutes on the shelf-life of gilthead seabream (Sparus aurata) fillets. *Aquaculture and Fisheries, 2*(1), 39–47. https://doi.org/10.1016/j.aaf.2016.10.003

Tsouko, E., Pilafidis, S., Dimopoulou, M., Kourmentza, K., & Sarris, D. (2023). Bioconversion of underutilized brewing by-products into bacterial cellulose by a newly isolated Komagataeibacter rhaeticus strain: A preliminary evaluation of the bioprocess environmental impact. *Bioresource Technology, 387*, Article 129667. https://doi.org/10.1016/j.biortech.2023.129667

Vanneste, J., Ennaert, T., Vanhulsel, A., & Sels, B. (2017). Unconventional pretreatment of lignocellulose with low-temperature plasma. *ChemSusChem, 10*(1), 14–31. https://doi.org/10.1002/cssc.201601381

Vieira, R. M., Gauthier, E., Widanagamage, G., McKenzie, N., Dunn, K., Moghaddam, L., Halley, P., & Brienzo, M. (2025). Uv-blocking and hydrophobicity improvement of chitosan-based film with lignin addition from a pilot scale-up Organosolv process of Banana pseudostem. *International Journal of Biological Macromolecules, 313*, Article 144254. https://doi.org/10.1016/j.ijbiomac.2025.144254

Vieira, E., Rocha, M. A. M., Coelho, E., Pinho, O., Saraiva, J. A., Ferreira, I. M., & Coimbra, M. A. (2014). Valuation of brewer's spent grain using a fully recyclable integrated process for extraction of proteins and arabinoxylans. *Industrial Crops and Products, 52*, 136–143. https://doi.org/10.1016/j.indcrop.2013.10.012

Wang, H.-M., Yuan, T.-Q., Song, G.-Y., & Sun, R.-C. (2021). Advanced and versatile lignin-derived biodegradable composite film materials toward a sustainable world. *Green Chemistry, 23*(11), 3790–3817. https://doi.org/10.1039/D1GC00790D

Yan, Q., Wang, L., Sun, X., Fan, F., Ding, J., Li, P., Zhu, Y., Xu, T., & Fang, Y. (2022). Improvement in the storage quality of fresh salmon (Salmo salar) using a powerful composite film of rice protein hydrolysates and chitosan. *Food Control, 142*, Article 109211. https://doi.org/10.1016/j.foodcont.2022.109211

Yin, Y., & Woo, M. W. (2024). Transitioning of petroleum-based plastic food packaging to sustainable bio-based alternatives. *Sustainable Food Technology, 2*(3), 548–566. https://doi.org/10.1039/D4FB00028E

Zadeh, E. M., O'Keefe, S. F., & Kim, Y.-T. (2018). Utilization of lignin in biopolymeric packaging films. *ACS Omega, 3*(7), 7388–7398. https://doi.org/10.1021/acsomega.7b01341

Zhang, Y., & Naebe, M. (2021). Lignin: A review on structure, properties, and applications as a light-colored UV absorber. *ACS Sustainable Chemistry & Engineering, 9*(4), 1427–1442. https://doi.org/10.1021/acssuschemeng.0c06998

Zhang, W., Shen, J., Gao, P., Jiang, Q., & Xia, W. (2022). Sustainable chitosan films containing a betaine-based deep eutectic solvent and lignin: Physicochemical, antioxidant, and antimicrobial properties. *Food Hydrocolloids, 129*, Article 107656. https://doi.org/10.1016/j.foodhyd.2022.107656

Zhang, X., Yang, M., Yuan, Q., & Cheng, G. (2019). Controlled preparation of corncob lignin nanoparticles and their size-dependent antioxidant properties: Toward high value utilization of lignin. *ACS Sustainable Chemistry & Engineering, 7*(20), 17166–17174. https://doi.org/10.1021/acssuschemeng.9b03535

Zolfaghari, S., Soltaninejad, A., Okoro, O. V., Shavandi, A., Denayer, J. F. M., Sadeghi, M., & Karimi, K. (2024). Starch biocomposites preparation by incorporating organosolv lignins from potato crop residues. *International Journal of Biological Macromolecules, 259*, Article 129140. https://doi.org/10.1016/j.ijbiomac.2023.129140